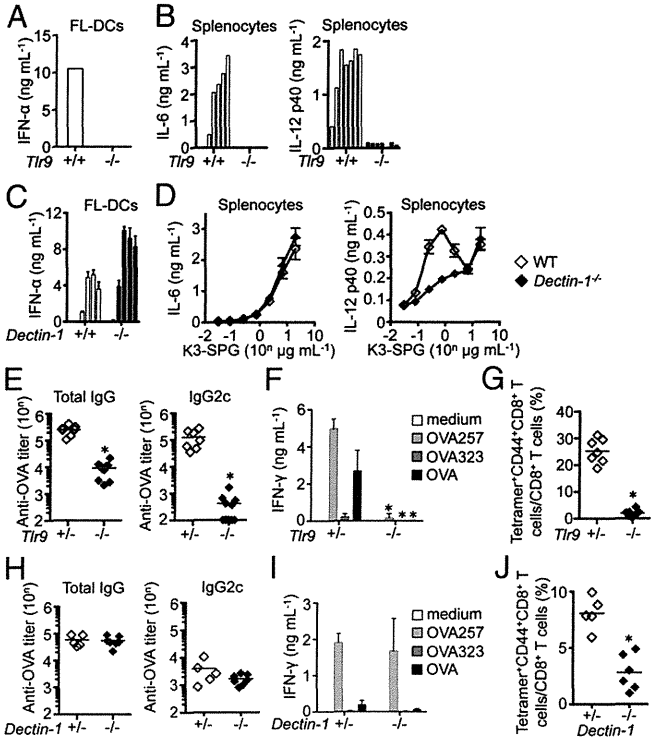

Fig. 4. Adjuvant effects of K3-SPG were completely dependent on TLR9 and partially on Dectin-1. FL-DCs (*A* and *C*) or splenocytes (*B* and *D*) from C57BL/6J, *Tlr9*$^{-/-}$, or *Dectin-1*$^{-/-}$ mice were stimulated with K3-SPG [20 μg/mL (*A*), 0.014–10 μg/mL (*B*), or 0.014–10 μg/mL (*C* and *D*)] for 24 h, and their cytokine production was monitored by ELISA. *Tlr9*$^{+/-}$ (n = 7) or *Tlr9*$^{-/-}$ mice (n = 10) (*E–G*) and *Dectin-1*$^{+/-}$ (n = 5) or *Dectin-1*$^{-/-}$ mice (n = 6) (*H–J*) were immunized s.c. with OVA (100 μg) and K3-SPG [10 μg (*E–G*) or 1 μg (*H–J*)] at days 0 and 10. Seven days after the last immunization, OVA-specific serum IgG (*E* and *H*), IFN-γ (*F* and *I*), and $OVA_{257-264}$-specific tetramer (*G* and *J*) were monitored. *$P < 0.05$ (Mann–Whitney *U* test). Data represent one of two or three independent experiments with similar results.

base of the tail, both antigen and adjuvant reached the surface of draining inguinal lymph nodes (iLNs) within 1 h (Fig. 5 *A*, *B*, and *D*). After 24 h, some K3-SPG had moved to the CD3e$^+$ T-cell area and colocalized with DQ-OVA (Fig. S6*A*). Those cells that contained both K3-SPG and DQ-OVA in the T-cell area of the iLNs were CD11c$^+$ DCs (Fig. S6*B*).

Of interest, the majority of fluorescence signals remained on the surface of the iLNs (Fig. 5*A*), prompting us to focus on two types of macrophages known to be distributed on the LN surface, Siglec-1$^+$ (also called CD169 or MOMA-1) macrophages (also known as subcapsular sinus macrophages) and MARCO$^+$ macrophages (31). Histological analysis using conventional fluorescence microscopy did not suitably reveal the entire iLN surface; moreover, these macrophages were difficult to isolate for flow cytometric analysis (32, 33). Hence, we used two-photon microscopy imaging analysis to clarify the distribution of antigen and K3-SPG ex vivo. After the injection of anti-MARCO and –Siglec-1 antibodies, specific macrophages were visualized (Movie S1). When the iLN surface was monitored by two-photon microscopy at 1 h postinjection, OVA and K3-SPG were colocalized with MARCO$^+$ but not Siglec-1$^+$ macrophages (Fig. 5 *B* and *D*, Fig. S7 *A–D*, and Movies 2–5). Previous reports suggest that the immune complex and inactivated influenza virus are captured by Siglec-1$^+$ macrophages to induce humoral immune responses (34, 35). The distribution pattern perfectly matched that for MARCO$^+$ macrophages in the iLNs and did not colocalize with Siglec-1$^+$ macrophages, as confirmed by Volocity's colocalization analysis (Perkin Elmer) (Fig. 5 *B–E*). In contrast, K3 was more diffusely distributed between MARCO$^+$ and Siglec-1$^+$ areas compared with K3-SPG (Fig. 5 *D* and *E*, Fig. S7 *C–E*, and Movies 6 and 7). Additionally, both *Tlr9*- and *Dectin-1*–deficient mice showed comparable localization of K3-SPG (Fig. S7 *F* and *G*).

To determine the contribution of these macrophages toward the adjuvant effects of K3-SPG, we examined different recovery kinetics of macrophages and DCs following an injection of clodronate liposomes into the base of the tail. After the injection, the macrophages were completely depleted by day 2. These cells did not recover for at least 1 wk, whereas DCs were mostly recovered by day 7, as previously reported (36). When both macrophages and DCs were depleted, immune responses were significantly suppressed [Fig. 5*F*, Clo (–d2)]. When only macrophages, but not DCs, were depleted, the immune responses were comparable to those in untreated mice [Fig. 5*F*, Clo (–d7)]. This would suggest that although both OVA and K3-SPG were mainly captured by

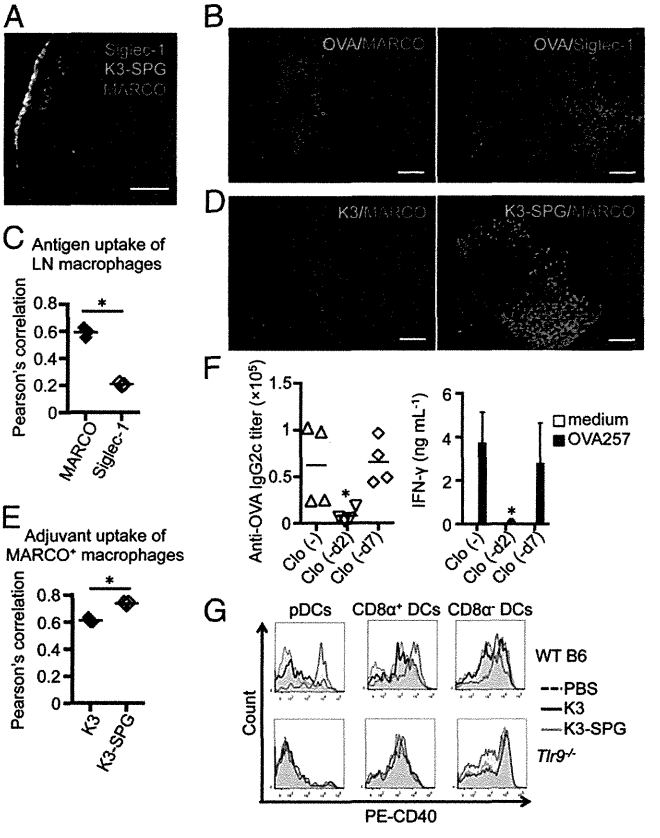

Fig. 5. Role of lymph node macrophages and dendritic cells in uptake and adjuvant effects of K3-SPG. (*A*) Immunohistochemistry of mouse inguinal LNs after Alexa 488-K3-SPG injection. One hour after injection, the LNs were collected and stained with anti–MARCO-phycoerythrin (PE) and anti–Siglec-1-APC antibodies. (*B–E*) Two-photon microscopic analysis of LNs. DQ-OVA, Alexa 488-K3, or Alexa 488-K3-SPG was injected as indicated, and anti–MARCO-PE or anti–Siglec-1-PE antibodies were administered. The LNs were collected 1 h later and analyzed by two-photon microscopy. (*C* and *E*) Colocalization of antigen or adjuvant with the stained macrophages was analyzed by Pearson's correlation. (*F*) Clodronate liposomes were injected into C57BL/6J mice either 2 or 7 d before immunization (n = 4). Mice were administered OVA (100 μg) plus K3-SPG (10 μg) at day 0. Eight days after immunization, OVA-specific serum IgG and IFN-γ were monitored. (*G*) C57BL/6J and *Tlr9*$^{-/-}$ mice were administered s.c. with K3 (10 μg) or K3-SPG (10 μg). At 24 h postadministration, the LNs were collected and the prepared cells were stained and analyzed by flow cytometry. (Scale bars, 100 μm.) *$P < 0.05$ (*t* test or Mann–Whitney *U* test). Data represent one of two or three independent experiments with similar results.

MARCO$^+$ macrophages in the LNs after injection, the macrophages were dispensable to inducing adaptive immune responses. In other words, the adjuvant effect of K3-SPG was largely dependent on the DC population.

K3-SPG Targets and Strongly Activates the Antigen-Bearing DC Population in Vivo. Our findings suggest that although a large portion of nanoparticulate K3-SPG was taken up by MARCO$^+$ macrophages in iLNs after injection, the adjuvant effects appear to be controlled by DCs. We focused on antigen and adjuvant uptake by the DC population in iLNs. At 24 h postinjection, the uptake of antigen and adjuvants by the DC population was analyzed by flow cytometry. The frequency of CpG-positives in three DC subsets (pDCs, CD8α$^+$ DCs, and CD8α$^-$ DCs) was significantly increased after K3-SPG injection than with K3 (Fig. S8*A*). In contrast, the frequency of OVA-positive DCs was comparable after K3 and K3-SPG injections (Fig. S8*B*). When we focused on both antigen- and adjuvant-positive DCs, there was a substantial increase for K3-SPG over K3 (Fig. S9). Both pDCs and CD8α$^+$ DCs in iLNs were strongly activated by K3-SPG but not by K3 24 h postinjection, and this was completely dependent on TLR9 (Fig. 5*G*). Our results indicate that pDCs and CD8α$^+$ DCs preferentially capture nanoparticulate K3-SPG rather than nonparticulate K3 for maturation and to exert adjuvant effects.

K3-SPG Is a Potent Adjuvant for Influenza Vaccine in Murine and Nonhuman Primate Models. Finally, we sought the adjuvant effect of K3-SPG by using more clinically relevant influenza vaccination models in both mice and nonhuman primates. When mice were immunized with ether-treated hemagglutinin antigen-enriched virion-free split vaccine (SV) plus the indicated adjuvant, K3-SPG demonstrated superior adjuvant effects to K3 when antibody responses (Fig. S10*A*) and T-cell responses (Fig. S10*B*) were compared. More importantly, SV plus K3-SPG immunization resulted in a 100-fold greater antibody response, even compared with vaccination using a whole (virion) inactivated vaccine (WIV) (0.2 μg per mouse) (Fig. 6*A*), which contains viral RNA as a built-in adjuvant (21). Interestingly, SV (0.1 μg per mouse) plus K3-SPG strongly induced both CD8 and CD4 T-cell responses (Fig. 6*B*). Mice immunized with SV and K3-SPG exhibited less body weight loss than WIV-immunized mice (Fig. 6*C*). Strikingly, K3-SPG conferred 100% protection against lethal PR8 virus challenge at the dose of which only 10% of WIV-vaccinated mice survived (Fig. 6*D*). These results strongly support the notion that K3-SPG works as a potent adjuvant for protein or protein-based vaccines in a murine model, prompting us to extend this finding to a nonhuman primate model using the cynomolgus monkey (*Macaca fascicularis*). Each group of three cynomolgus monkeys was immunized with SV plus K3 or K3-SPG at days 0 and 14. Serum antibody titers were then monitored for 8 wk. The SV plus K3-SPG induced significantly higher antibody titer at 2 wk postimmunization, and titer levels remained high for at least another 6 wk (Fig. 6*E*). Although antibody titers were reduced at 110 wk after immunization, the K3-SPG group had higher antibody titers than the K3 group (Fig. 6*E*). When PBMCs were stimulated with SV and WIV, IFN-γ was detected from the SV plus K3-SPG–immunized group (Fig. 6*F*). Taken together, these results suggest that K3-SPG is a prominent vaccine adjuvant in a nonhuman primate model.

Discussion

The medical need for novel, potent, and safe adjuvants is ever-increasing these days as (*i*) recombinant vaccine antigens such proteins and peptides are short on natural adjuvants, unlike attenuated or inactivated whole microbial antigens, (*ii*) conventional aluminum salts and oil adjuvants are limited or preferred for enhancing humoral immune responses, and (*iii*) new adjuvants that can induce cellular immune responses, including CTLs, are needed, for example for cancer vaccines. The last two decades have resulted in tremendous progress with respect to adjuvant research and development. A hallmark of the new generation of adjuvants is that nucleic acids have been rediscovered to be immunologically active in stimulating specific innate immune receptors of the host, in particular TLRs. CpG DNA, a ligand for TLR9, is one of the most promising immunotherapeutic agents that has been identified.

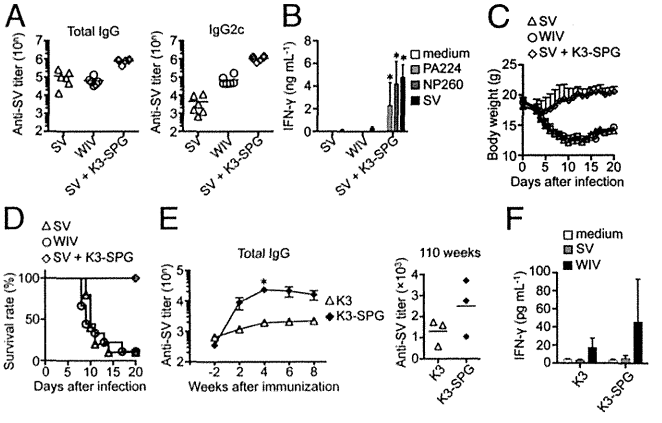

Fig. 6. K3-SPG acts as an influenza vaccine adjuvant in mice and nonhuman primates. (*A–D*) C57BL/6J mice (n = 6 or 10) were immunized with SV (0.1 μg), whole inactivated vaccine (WIV) (0.2 μg), or SV (0.1 μg) plus K3-SPG (10 μg) at days 0 and 14. Seven days after the final immunization, SV-specific serum IgG titers (*A*) and IFN-γ (*B*) [specific to SV antigen, $PA_{224-233}$ (PA224) (10 μg/mL) or $NP_{260-283}$ (NP260)] were monitored. (*C* and *D*) Fourteen days after the final immunization, mice were challenged with a 10-LD_{50} dose of influenza virus A/PR/8 (H1N1). Changes in body weights (*C*) and mortality (*D*) were monitored for the next 20 d. (*E* and *F*) Cynomolgus monkeys (n = 3) were immunized with SV (5 μg) plus K3 (5 nmol) or SV plus K3-SPG (5 nmol) at days 0 and 14. (*E*) Serum samples were collected at −2, 2, 4, 6, 8, and 110 wk. Antigen-specific serum antibody titers were measured by ELISA. (*F*) PBMCs were prepared from individual cynomolgus monkey blood at 4 wk after the first immunization and restimulated in vitro with medium, SV (10 μg), or WIV for 24 h. Mouse IFN-γ in the supernatants was determined by ELISA. *P < 0.05 (t test or Mann–Whitney U test).

Although there are several types of potent humanized CpG ODN—K (also called B), D (A), C, and P types—the development of an all-in-one CpG ODN activating both B cells and pDCs to form a stable nanoparticle without aggregation has been less than successful. In this study, we generated a novel K CpG ODN that we designated K3-SPG. Although it had been reported that there are molecular interactions between single-stranded nucleic acids and β-glucan (37) and that murine and humanized CpG ODNs can be wrapped by SPG to increase their original TLR9-agonistic activities (20), our report demonstrates that a rod-shaped nano-sized K3-SPG particle exhibits dual characteristics of K and D CpG ODNs (Fig. 1). K3-SPG is distinct from other previously reported K CpG ODNs, including K3. In turn, K3-SPG becomes a D CpG ODN, stimulating human PBMCs to produce large amounts of both type I and type II IFN, targeting the same endosome where the IFN-inducing D type resides without losing its K-type activity (Fig. 1 *F* and *G*). Another surprising finding is that this K3-SPG forms a rod-like single nanomolecule (Fig. 1 *C* and *D*). This is advantageous over previously demonstrated D or P types, whose ends form higher-order structures that may hamper further development as prodrugs, including good manufacturing practice assignment.

Another prominent feature of this K3-SPG is its potency as an adjuvant for induction of both humoral and cellular immune responses, especially CTL induction, to coadministered protein antigens without conjugation. Such potent adjuvant activity of K3-SPG is attributable to its nanoparticulate nature (Figs. 1 *C* and *D* and 2) rather than targeting Dectin-1 by SPG (Figs. 3 and 4). Initially, we hypothesized that K3-SPG becomes such a potent adjuvant because it targets Dectin-1, because SPG is a β-1,3-glucan, and seems to be a clear Dectin-1 ligand (Fig. 3*A*). Our other results, however, led us to conclude that the role of Dectin-1

in vivo with respect to the adjuvant activity of K3-SPG was minimal (Fig. 4). More importantly, the in vivo activity of K3-SPG was completely dependent upon TLR9 (Fig. 4 *E–G*). SPG is a soluble Dectin-1 ligand but not a Dectin-1 agonist, and thus does not interfere with TLR9-mediated DC activation (Fig. 3 *D* and *E*). The adjuvant activity of K3-SPG is mostly independent of Dectin-1, except at very low doses during the immunization protocol (Fig. 4*J*). Instead, some other receptors such as C-type lectins, Siglecs, and scavenger receptors may play roles in delivering SPG into macrophages and/or DCs, accumulating and activating antigen-bearing macrophages and DCs in draining lymph nodes (Fig. 5). In this regard, we also found that $MARCO^+$, but not Siglec-1^+, macrophages in draining lymph nodes are dominant in capturing K3-SPG, and coadministered antigen (LPS-free OVA protein), and that K3-SPG targets the antigen-bearing DC population in vivo. Although the depletion of macrophages did not ameliorate adjuvant effects, large amounts of antigen and K3-SPG are taken up by the same $MARCO^+$ macrophages, and the two-photon microscopic data suggest that they are activated as they become much bigger than nonstimulated macrophages. Whether this massive accumulation of antigen and adjuvant in $MARCO^+$ macrophages contributes to the following DC activation and adaptive T- and B-cell activation is yet to be elucidated in future work.

The protective potency of K3-SPG as an influenza vaccine adjuvant was demonstrated in vivo in both murine and nonhuman primate models. In the murine model, intradermal immunization with a very low dose of seasonal influenza split vaccine mixed with K3-SPG in solution provoked robust IgG responses and offered better protection than a low but physiological dose of whole inactivated virion vaccination against the heterologous challenge of lethal virus (Fig. 6 *C* and *D*). These data provide better protective potency than our previous results, where we used approximately 10 times higher doses of influenza antigens (21), because many factors for K3-SPG have been improved for its potency: K3–SPG complexation efficiency and optimization of the order between K3 and poly(dA_{40}) (Fig. 1); the immunization route is different as well. The data above prompted us to develop K3-SPG as a potent adjuvant for influenza split vaccine, especially for those urgently needing improvement: seasonal influenza vaccination for the elderly, immunodeficient patients (transplant recipients), and pandemic influenza vaccination.

Taken together, these data suggest that K3-SPG can be used as a potent adjuvant for protein vaccines such as influenza split vaccines, and may be useful for immunotherapeutic applications that require type I and type II IFN as well as CTL induction.

Materials and Methods

All animal studies using mice and monkeys were conducted in accordance with the Institutional Animal Care and Use Committee at the National Institute of Biomedical Innovation. All of the ODNs used in this manuscript were synthesized by GeneDesign. Other details are described in *SI Materials and Methods*.

ACKNOWLEDGMENTS. This study was supported by a Health and Labour Sciences Research Grant and the Japan Science and Technology Agency Core Research for Evolutionary Science and Technology Program.

1. Hemmi H, et al. (2000) A Toll-like receptor recognizes bacterial DNA. *Nature* 408(6813):740–745.
2. Krieg AM (2006) Therapeutic potential of Toll-like receptor 9 activation. *Nat Rev Drug Discov* 5(6):471–484.
3. Chu RS, Targoni OS, Krieg AM, Lehmann PV, Harding CV (1997) CpG oligodeoxynucleotides act as adjuvants that switch on T helper 1 (Th1) immunity. *J Exp Med* 186(10):1623–1631.
4. Brazolot Millan CL, Weeratna R, Krieg AM, Siegrist CA, Davis HL (1998) CpG DNA can induce strong Th1 humoral and cell-mediated immune responses against hepatitis B surface antigen in young mice. *Proc Natl Acad Sci USA* 95(26):15553–15558.
5. Klinman DM (2004) Immunotherapeutic uses of CpG oligodeoxynucleotides. *Nat Rev Immunol* 4(4):249–258.
6. Vollmer J, Krieg AM (2009) Immunotherapeutic applications of CpG oligodeoxynucleotide TLR9 agonists. *Adv Drug Deliv Rev* 61(3):195–204.
7. Krug A, et al. (2001) Identification of CpG oligonucleotide sequences with high induction of IFN-alpha/beta in plasmacytoid dendritic cells. *Eur J Immunol* 31(7): 2154–2163.
8. Verthelyi D, Ishii KJ, Gursel M, Takeshita F, Klinman DM (2001) Human peripheral blood cells differentially recognize and respond to two distinct CpG motifs. *J Immunol* 166(4):2372–2377.
9. Hartmann G, Krieg AM (2000) Mechanism and function of a newly identified CpG DNA motif in human primary B cells. *J Immunol* 164(2):944–953.
10. Hartmann G, et al. (2003) Rational design of new CpG oligonucleotides that combine B cell activation with high IFN-alpha induction in plasmacytoid dendritic cells. *Eur J Immunol* 33(6):1633–1641.
11. Marshall JD, et al. (2003) Identification of a novel CpG DNA class and motif that optimally stimulate B cell and plasmacytoid dendritic cell functions. *J Leukoc Biol* 73(6):781–792.
12. Samulowitz U, et al. (2010) A novel class of immune-stimulatory CpG oligodeoxynucleotides unifies high potency in type I interferon induction with preferred structural properties. *Oligonucleotides* 20(2):93–101.
13. Kerkmann M, et al. (2005) Spontaneous formation of nucleic acid-based nanoparticles is responsible for high interferon-alpha induction by CpG-A in plasmacytoid dendritic cells. *J Biol Chem* 280(9):8086–8093.
14. Klein DC, Latz E, Espevik T, Stokke BT (2010) Higher order structure of short immunostimulatory oligonucleotides studied by atomic force microscopy. *Ultramicroscopy* 110(6):689–693.
15. Puig M, et al. (2006) Use of thermolytic protective groups to prevent G-tetrad formation in CpG ODN type D: Structural studies and immunomodulatory activity in primates. *Nucleic Acids Res* 34(22):6488–6495.
16. McHutchison JG, et al. (2007) Phase 1B, randomized, double-blind, dose-escalation trial of CPG 10101 in patients with chronic hepatitis C virus. *Hepatology* 46(5): 1341–1349.
17. Bode C, Zhao G, Steinhagen F, Kinjo T, Klinman DM (2011) CpG DNA as a vaccine adjuvant. *Expert Rev Vaccines* 10(4):499–511.
18. Okamura K, et al. (1986) Clinical evaluation of schizophyllan combined with irradiation in patients with cervical cancer. A randomized controlled study. *Cancer* 58(4): 865–872.
19. Sakurai K, Mizu M, Shinkai S (2001) Polysaccharide—polynucleotide complexes. 2. Complementary polynucleotide mimic behavior of the natural polysaccharide schizophyllan in the macromolecular complex with single-stranded RNA and DNA. *Biomacromolecules* 2(3):641–650.
20. Shimada N, et al. (2007) A polysaccharide carrier to effectively deliver native phosphodiester CpG DNA to antigen-presenting cells. *Bioconjug Chem* 18(4):1280–1286.
21. Koyama S, et al. (2010) Plasmacytoid dendritic cells delineate immunogenicity of influenza vaccine subtypes. *Sci Transl Med* 2(25):25ra24.
22. Minari J, et al. (2011) Enhanced cytokine secretion from primary macrophages due to Dectin-1 mediated uptake of CpG DNA/β-1,3-glucan complex. *Bioconjug Chem* 22(1):9–15.
23. Bae AH, et al. (2004) Rod-like architecture and helicity of the poly(C)/schizophyllan complex observed by AFM and SEM. *Carbohydr Res* 339(2):251–258.
24. Costa LT, et al. (2004) Structural studies of oligonucleotides containing G-quadruplex motifs using AFM. *Biochem Biophys Res Commun* 313(4):1065–1072.
25. Gürsel M, Verthelyi D, Gürsel I, Ishii KJ, Klinman DM (2002) Differential and competitive activation of human immune cells by distinct classes of CpG oligodeoxynucleotide. *J Leukoc Biol* 71(5):813–820.
26. Guiducci C, et al. (2006) Properties regulating the nature of the plasmacytoid dendritic cell response to Toll-like receptor 9 activation. *J Exp Med* 203(8):1999–2008.
27. Herre J, et al. (2004) Dectin-1 uses novel mechanisms for yeast phagocytosis in macrophages. *Blood* 104(13):4038–4045.
28. Goodridge HS, et al. (2011) Activation of the innate immune receptor Dectin-1 upon formation of a 'phagocytic synapse.' *Nature* 472(7344):471–475.
29. Eberle ME, Dalpke AH (2012) Dectin-1 stimulation induces suppressor of cytokine signaling 1, thereby modulating TLR signaling and T cell responses. *J Immunol* 188(11):5644–5654.
30. Saijo S, et al. (2007) Dectin-1 is required for host defense against *Pneumocystis carinii* but not against *Candida albicans*. *Nat Immunol* 8(1):39–46.
31. Martinez-Pomares L, Gordon S (2012) $CD169^+$ macrophages at the crossroads of antigen presentation. *Trends Immunol* 33(2):66–70.
32. Aoshi T, et al. (2009) The cellular niche of *Listeria monocytogenes* infection changes rapidly in the spleen. *Eur J Immunol* 39(2):417–425.
33. Gray EE, Cyster JG (2012) Lymph node macrophages. *J Innate Immun* 4(5-6):424–436.
34. Suzuki K, Grigorova I, Phan TG, Kelly LM, Cyster JG (2009) Visualizing B cell capture of cognate antigen from follicular dendritic cells. *J Exp Med* 206(7):1485–1493.
35. Gonzalez SF, et al. (2010) Capture of influenza by medullary dendritic cells via SIGN-R1 is essential for humoral immunity in draining lymph nodes. *Nat Immunol* 11(5): 427–434.
36. Aoshi T, et al. (2008) Bacterial entry to the splenic white pulp initiates antigen presentation to $CD8^+$ T cells. *Immunity* 29(3):476–486.
37. Sakurai K, Shinkai S (2000) Phase separation in the mixture of schizophyllan and poly (ethylene oxide) in aqueous solution driven by a specific interaction between the glucose side chain and poly(ethylene oxide). *Carbohydr Res* 324(2):136–140.

OPEN ACCESS Freely available online

PLOS | ONE

Effects of Mycobacteria Major Secretion Protein, Ag85B, on Allergic Inflammation in the Lung

Yusuke Tsujimura[1], Hiroyasu Inada[2], Misao Yoneda[3], Tomoyuki Fujita[4], Kazuhiro Matsuo[5], Yasuhiro Yasutomi[1,6]*

1 Laboratory of Immunoregulation and Vaccine Research, Tsukuba Primate Research Center, National Institute of Biomedical Innovation, Tsukuba, Ibaraki, Japan, **2** Department of Pharmaceutical Sciences, Suzuka University of Medical Science, Suzuka, Mie, Japan, **3** Department of Pathologic Oncology, Institute of Molecular and Experimental Medicine, Faculty of Medicine, Mie University Graduate School of Medicine, Tsu, Mie, Japan, **4** Research Laboratories, Kyoto R&D Center, Maruho Co., Ltd, Chudoji, Shimogyo-ku, Kyoto, Japan, **5** Research and Development Department, Japan BCG Laboratory, Kiyose, Tokyo, Japan, **6** Department of Immunoregulation, Mie University Graduate School of Medicine, Tsu, Mie, Japan

Abstract

Many epidemiological studies have suggested that the recent increase in prevalence and severity of allergic diseases such as asthma is inversely correlated with *Mycobacterium bovis* bacillus Calmette Guerin (BCG) vaccination. However, the underlying mechanisms by which mycobacterial components suppress allergic diseases are not yet fully understood. Here we showed the inhibitory mechanisms for development of allergic airway inflammation by using highly purified recombinant Ag85B (rAg85B), which is one of the major protein antigens secreted from *M. tuberculosis*. Ag85B is thought to be a single immunogenic protein that can elicit a strong Th1-type immune response in hosts infected with mycobacteria, including individuals vaccinated with BCG. Administration of rAg85B showed a strong inhibitory effect on the development of allergic airway inflammation with induction of Th1-response and IL-17and IL-22 production. Both cytokines induced by rAg85B were involved in the induction of Th17-related cytokine-production innate immune cells in the lung. Administration of neutralizing antibodies to IL-17 or IL-22 in rAg85B-treated mice revealed that IL-17 induced the infiltration of neutrophils in BAL fluid and that allergen-induced bronchial eosinophilia was inhibited by IL-22. Furthermore, enhancement of the expression of genes associated with tissue homeostasis and wound healing was observed in bronchial tissues after rAg85B administration in a Th17-related cytokine dependent manner. The results of this study provide evidence for the potential usefulness of rAg85B as a novel approach for anti-allergic effect and tissue repair other than the role as a conventional TB vaccine.

Citation: Tsujimura Y, Inada H, Yoneda M, Fujita T, Matsuo K, et al. (2014) Effects of Mycobacteria Major Secretion Protein, Ag85B, on Allergic Inflammation in the Lung. PLoS ONE 9(9): e106807. doi:10.1371/journal.pone.0106807

Editor: Yoshihiko Hoshino, National Institute of Infectious Diseases, Japan

Received April 18, 2014; **Accepted** August 6, 2014; **Published** September 5, 2014

Data Availability: The authors confirm that all data underlying the findings are fully available without restriction. All relevant data are within the paper and its Supporting Information files.

Funding: This work was supported by Health Science Research Grants from the Ministry of Health, Labor, and Welfare of Japan and the Ministry of Education, Culture, Sports, Science, and Technology of Japan. The funders had no role in study design, data collection and analysis, decision to publish, or preparation of the manuscript.

Competing Interests: The authors have no commercial or financial conflict of interest. The authors also have no competing interest in Maruho Co., Ltd. This does not alter the authors' adherence to PLOS ONE policies on sharing data and materials.

* Email: yasutomi@nibio.go.jp

Introduction

Epidemiological studies showed that treatments with bacterial and viral products might be effective therapeutic strategies for suppressing the development of allergic responses [1–3]. Administration of mycobacteria, including *Mycobacterium bovis*-Bacillus Calmette Guerin (BCG), has been thought to be effective for preventing the development of asthma by induction of Th1-type immune responses [4], regulatory T (Treg) cells [5,6] and NKT cells [7,8]. On the other hand, recent data have revealed that *Mycobacterium tuberculosis* infection induced not only IFN-γ but also IL-17, which promotes granuloma organization followed by neutrophil recruitment, and IL-22, which promotes regeneration and protects against tissue damage [9]. In addition, vaccination with the mycobacteria-secreted immunogenic protein Ag85A had important links with Th1/Th17 cell induction and Treg cell reduction [10]. However, the role of mycobacteria-mediated Th17-related cytokines in allergic asthma remains unknown.

The airway epithelium and innate immune cells are considered to be essential controllers of inflammatory, immune and regenerative responses to allergens that contribute to asthma pathogenesis [11]. Dysfunction of the epithelium leading to chronic injury was suggested to be a consequence of sustained airway inflammation that is associated with Th2-driven adaptive immunity [12]. Tissue homeostasis at exposed surfaces of the lung is regulated by Th17-related cytokines, especially IL-22, in the innate immune system [13]. Therefore, the functional and structural maintenance of tissue might be necessary to induce both innate and adaptive immunity.

One immunogenic protein that can induce a strong Th1-type immune response in hosts sensitized by BCG is thought to be Ag85B. Ag85B is one of the most dominant protein antigens secreted from all mycobacterial species and has been shown to

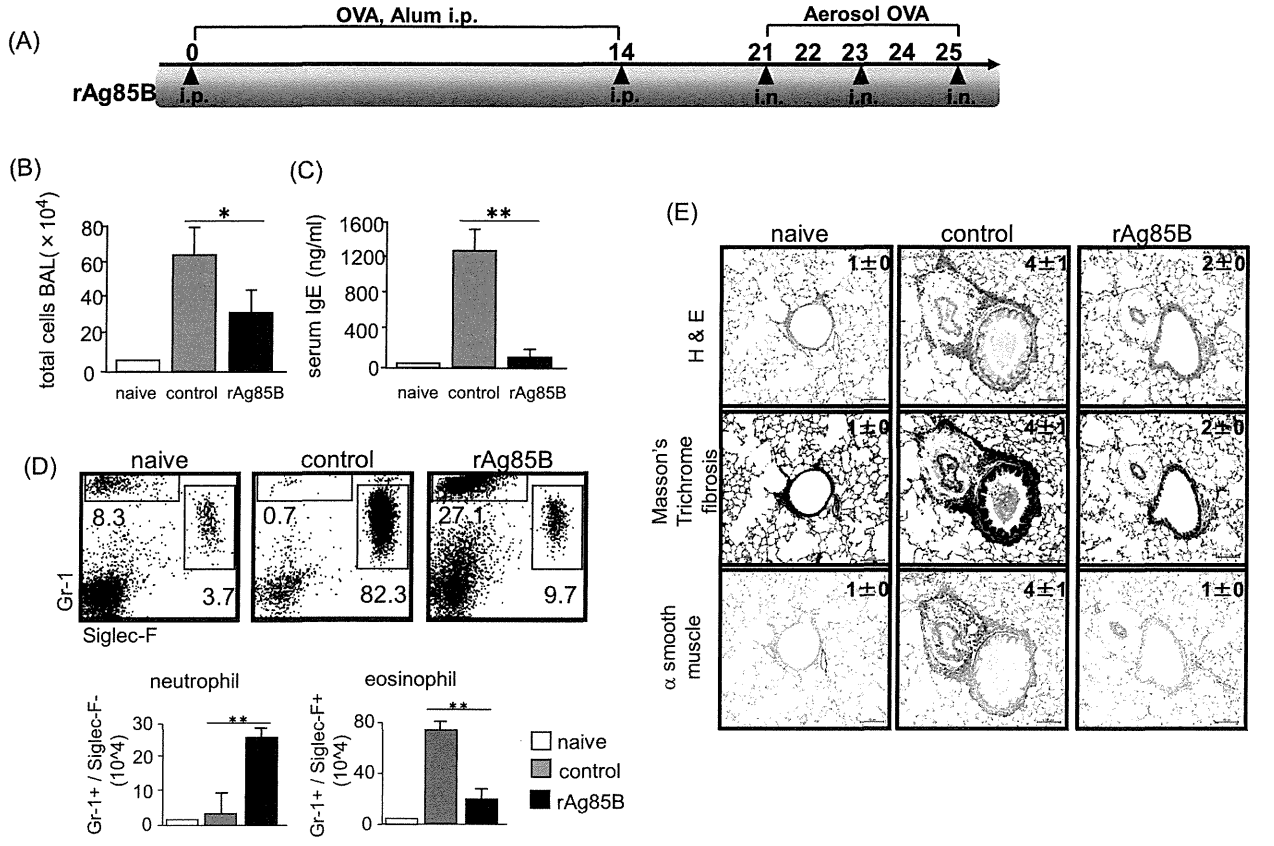

Figure 1. Functions of rAg85B in allergic inflammation. Experimental design used to investigate the effects of rAg85B on OVA-induced allergic lung inflammation (*A*). BALB/c mice were intraperitoneally immunized with OVA on days 0 and 14. On days 21 to 25 after the first immunization, mice were exposed to aerosolized 5% OVA for 20 min. Three hours prior to OVA inhalation, the mice were i.p. (100 μg; days 0 and 14) and i.n. (20 μg; days 21, 23, and 25) administered rAg85B. One day after the last challenge, the BAL cells were counted (*B*) and OVA-specific serum IgE concentrations were determined by ELISA (*C*). Flow cytometry of BAL cells from naïve or OVA sensitized BALB/c mice treated with PBS or rAg85B, stained with anti-Gr-1 and anti-Siglec-F. Numbers adjacent to outlined area indicate percent of eosinophils (Gr-1^{dull}, Siglec-F^{+}), and neutrophils (Gr-1^{+}, Siglec-F^{neg}) (*D*). Formalin-fixed tissue sections were stained with hematoxylin and eosin to visualized cell recruitment (upper row, scale bar, 100 mm), Masson's trichrome (center row, scale bar, 100 mm), and α-smooth muscle actin (lower row, scale bar, 50 mm). Numbers in quadrants indicate the score scale from 0 to 5 in each. (*E*). Data are representative of at least three independent experiments. (*P<0.05, **P<0.01 compared with OVA control. error bars, s.d.; n = 6 mice).
doi:10.1371/journal.pone.0106807.g001

induce substantial Th cell proliferation and vigorous Th1 cytokine production in humans and mice [14]. In addition, we have reported the possibility of using Ag85B DNA as an immunological strategic tool to induce both Th1 and Treg cells in immunotherapy for atopic dermatitis and allergic asthma [15,16].

In the present study, we found that highly purified recombinant Ag85B protein (rAg85B) had suppressive effects depending on induction of Th1 immune responses in a mouse model of allergic lung inflammation. Remarkably, rAg85B administration also promoted IL-17 and IL-22 production in both Th17 cells in lymph nodes (LNs) and various innate immune cells such as gamma delta T (γδT) cells, NKp46^{+} cells, lymphoid tissue inducer (LTi)-like cells, and CD11c^{+} cells in BAL fluid. More interestingly, Th17-related cytokines induced by rAg85B were involved in enhancement of the expression of genes related to maintenance of tissue homeostasis. This is the first report demonstrating that mycobacteria major secreting protein Ag85B plays an important role in the regulation of allergic airway inflammation by inducing not only a Th1-response but also recruitment of an IL-17 and/or IL-22-producing Th cell subset in LNs and innate immune BAL cells in a manner dependent on Th17-related cytokines in order to retain tissue integrity.

Materials and Methods

Animal and Ethic Statement

Specific pathogen-free BALB/c mice (six-week-old, female) were purchased from CLEA Japan. All of the experiments in this study were performed in accordance with the Guidelines for Animal Use and Experimentation, as set out by the National Institute of Biomedical Innovation. The protocol was approved by the Animal Welfare and Animal Care Committee of the National Institute of Biomedical Innovation (Permit Number: DS23-8R2). All animal procedures were used to minimize animal pain and suffering.

Experimental protocol

BALB/c mice were intraperitoneally immunized with 10 μg ovalbumin (OVA) with 1 mg aluminum hydroxide on days 0 and 14. On days 21 to 25 after the first immunization, mice were exposed to aerosolized 5% OVA for 20 min. Three hours prior to

OVA inhalation, the mice were intraperitoneally (i.p.) (100 μg; days 0 and 14) and intranasal ly (i.n.) (20 μg; days 21, 23, and 25) administered rAg85B. OVA-sensitized Balb/c mice were challenged intranasally with PBS, rAg85B, rAg85B plus 5 μg anti-IL-17 Abs and/or 10 μg anti-IL-22 Abs (R&D Systems) with the same time course as that of rAg85B i.n. administration. The isotype-matched control antibody for neutralization experiments was set using normal goat IgG control (R&D systems).

Recombinant protein Ag85B production

Plasmids containing the Ag85B gene were transformed into *E. coli* TG1. The expressed inclusion body (IB) was harvested from the disrupted cell pellet by a homogenizer with lysis buffer (30 mM sodium phosphaste, 100 mM NaCl, 5 mM EDTA and 0.5% Triton X-100). This IB of Ag85B was unfolded in 8 M urea and refolded by dilution to 0.4 M urea. The urea in the refolding buffer was removed by anion exchange chromatography using 20 mM Tris buffer and 20 mM Tris buffer with 1 M NaCl (pH 8.5). The refolded Ag85B was loaded on a cation exchange column, and crude Ag85B was passed through the resin using 50 mM NaOAc buffer and 50 mM NaOAc buffer with 1 M NaCl (pH 6.0). Finally, Ag85B was purified by anion exchange chromatography using 20 mM Tris buffer and 20 mM Tris buffer with 1 M NaCl (pH 7.6).

Endotoxin test

The endotoxin value of Ag85B was measured by Kinetic turbidimetric LAL assay kit (Lonza). Test was carried out according to the manufacture's instruction. The endotoxin value was measured kinetically on ELISA after mixing sample and LAL reagent and was calculated automatically according to standard curve. Purified Ag85B had a purity of >95% analyzed by SDS-PAGE and contaminated less than 0.02 EU/mg of endotoxin. Protein quantitation was carried out by UV spectroscopy at 280 nm.

Isolation and analysis of lymph node and BAL cells

BAL cells were prepared according to a published protocol [16]. Single cell suspensions from BAL fluid and mediastinal lymph nodes (MLNs) were obtained by crushing through cell strainers. Cells were stained with antibodies to the following markers: CD3, CD4, CD8, CD19, CD11b, CD11c, CD25, γδ TCR, NKp46, Gr-1, Siglec-F, CD127, IFN-γ, IL-4, Foxp3, IL-17 and IL-22 (BD). For analysis of intracellular cytokine production, cells were stimulated directly by incubation for 5 h with 50 ng/ml PMA and 750 ng/ml ionomycin (Sigma-Aldrich) at 37°C and with 10 μg/ml brefeldin A (eBioscience) added in the last 3 h. Flow cytometry data collection was performed on a FACS Calibur (BD). Files were analyzed using CellQuest Software (BD).

Quantification of cytokines and chemokines

Concentrations of cytokines and chemokines in BAL fluid and culture supernatants of OVA-restimulated lymph node cells were determined by ELISA using commercial kits from R&D Systems. Twenty-four hours after the last OVA sensitization, MLNs and BAL fluid were harvested. MLNs were cultured with 50 μg/ml OVA, and cytokines in the culture supernatant were determined 48 h after incubation. The BAL fluid were measured directly.

Lung histology

The organs were removed and placed in 4% buffered paraformaldehyde (PFA) overnight. Excess paraformaldehyde was removed by incubation in fresh PBS. Fixed tissues were incubated at 4°C in 70% ethanol. PFA-fixed lung sections were stained with hematoxylin and eosin, Masson's trichrome, and α-smooth muscle actin. Peribronchial infiltrates, fibrosis, and smooth muscle hyperplasia were assessed by a semiquantitative score (0–5) by a pathologist.

Quantitative real-time PCR

RNA was isolated from whole lung tissue using mechanical homogenization and TRIzol reagent (Invitrogen) according to the manufacturer's instructions. RNA concentrations were measured with a Nanodrop ND 1000 (Nucliber). Omniscript reverse tanscriptase was used according to the protocol of the manufacturer (QIAGEN) for the production of cDNA in a reaction volume of 20 ul. Primers for quantitative real-time RT-PCR were designed with the Universal ProbeLibrary Assay Design Center (Roche Applied Science). Reactions were run on an RT-PCR system (LightCycler 480; Roche Applied Science) Samples were normalized to b-actin and displayed as fold induction over naïve or untreated controls unless otherwise stated.

TLR/NLR ligand screening

The presence of TLR and NLR ligands were tested on recombinant human embryonic kidney 293 (HEK293) cell lines

Table 1. Effects of rAg85B to Toll-Like and NOD-Like Receptor.

receptor	No ligand	rAg85B	control (+)
mTLR2	0.1±0.0	0.1±0.0	2.3±0.1
mTLR3	0.1±0.0	0.1±0.0	2.4±0.2
mTLR4	0.1±0.0	0.1±0.0	2.7±0.1
mTLR5	0.1±0.0	0.1±0.0	2.7±0.1
mTLR7	0.1±0.0	0.1±0.0	2.1±0.0
mTLR8	0.1±0.0	0.1±0.0	2.3±0.1
mTLR9	0.1±0.0	0.1±0.0	2.6±0.1
mNOD1	0.1±0.0	0.1±0.0	1.7±0.1
mNOD2	0.2±0.0	0.1±0.0	1.6±0.1

The results are provided as optical density values (650 nm).
The values represent the means and standard deviations of three screenings.
TLR/NLR ligand screening were performed by InvivoGen, as described in Methods.
doi:10.1371/journal.pone.0106807.t001

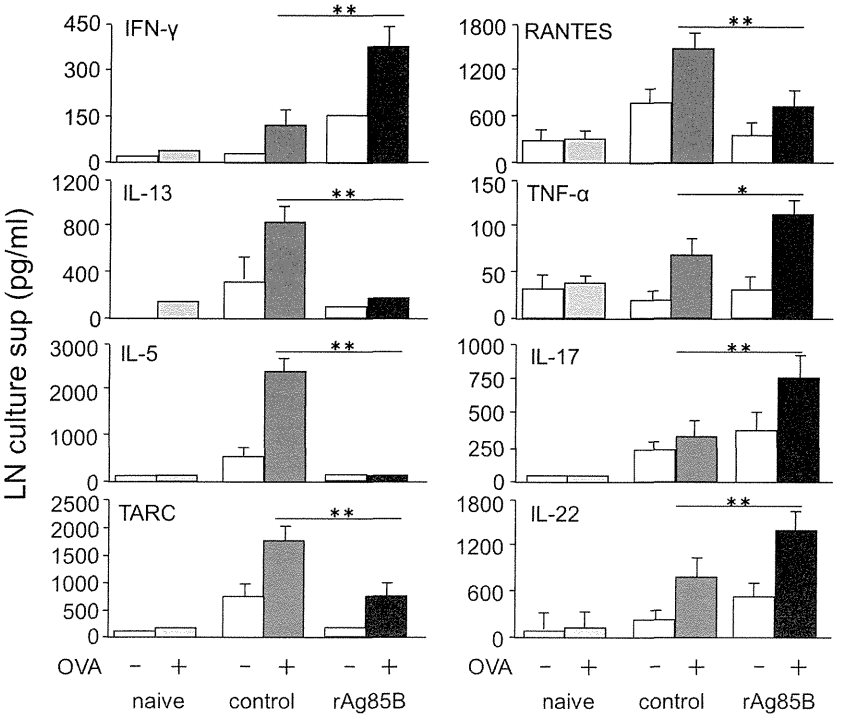

Figure 2. Administaration of rAg85B induced immune deviation from a Th2-response towards a Th1, Th17-related response in OVA-stimulated LN cells. OVA-immunized (i.p., day0 and 14) and sensitized (5% aerosolized-OVA, day21 to 25) BALB/c mice were challenged with PBS or rAg85B protein (i.p. (100 μg; days 0 and 14) and i.n. (20 μg; days 21, 23, and 25)). At 24 h after the last OVA sensitization, mediastinal lymph nodes (MLNs) from naïve or OVA sensitized BALB/c mice treated with PBS or rAg85B, were harvested. MLNs were cultured with OVA (50 μg/ml), and cytokines in the culture supernatant were determined 48 h after incubation by ELISA. Data are representative of at least three independent experiments (*P<0.05, **P<0.01 compared with OVA control. error bars, s.d.; n = 6 mice).
doi:10.1371/journal.pone.0106807.g002

which utilize a nuclear factor-kB inducible SEAP (secreted embryonic alkaline phosphatase) reporter gene as the read-out. These HEK293-derived cells are functionally expressing a given TLR or NOD gene from human or mouse. A recombinant HEK293 cell line for the reporter gene only was used as negative control. Positive control ligands are heat-killed *Listeria monocytogenes* (HKLM) for TLR2, Poly(I:C) for TLR3, Lipopolysaccharide (LPS); K12 for TLR4, Flagellin for TLR5, CL097 for TLR7, CL075 and poly(dT) for TLR8, CpG ODN for TLR9, C12-iEDAP for NOD1, and L18-MDP for NOD2. rAg85B (10 μg/mL) was added to the reaction volume. TLR/NLR ligand screening were performed by InvivoGen.

Statistical analysis

Data are shown as means±SD. Statistical significance of differences between the OVA-control group and rAg85B-treated group was assessed by the non-parametric Mann-Whitney U-test. Statistical comparisons between groups of rAg85B+isotype control and rAg85B+neutralization antibody were performed using the non-paramatric Kruskal-Wallis H-test.

Results

Effects on allergic inflammation by administration of rAg85B

To investigate the role of rAg85B in pulmonary allergic inflammation, we examined the frequently used mouse model of ovalbumin (OVA)-induced allergic lung inflammation. The mice were intraperitoneally (i.p.) (days 0 and 14) and intranasally (i.n.) (days 21, 23, and 25) administered with rAg85B (Fig. 1*A*). The purity of rAg85B was evaluated by silver staining of SDS-PAGE gel (Fig. S1) and the Limulus Amebocyte Lysate (LAL) assay (less than 0.02 EU (endotoxin units)/ml). Furthermore rAg85B was not contaminated with any TLR/NLR binding immune stimulants (Table 1). Twenty-four hours after the final OVA challenge, inflammatory cell recruitment into the lungs was analyzed. The OVA-induced allergic manifestation was suppressed with a decrease in the total number of bronchoalveolar lavage (BAL) cells and serum IgE level in the rAg85B-administered mice (Fig. 1*B*, *1C*). A marked reduction in eosinophil (Gr-1(+)/Siglec-F(+)) infiltration was observed by flow cytometric (FACS) analysis of BAL in rAg85B-administered mice (Fig. 1*D*). In association with decreased eosinophilia, neutrophil (Gr-1(+)/Siglec-F(-)) recruitment was seen in rAg85B-administered mice (Fig. 1*D*). These results were confirmed by histopathological observation of hematoxylin and eosin (H&E) staining (Fig. 1*E*). Mice administered rAg85B showed inhibition of infiltration of cells. (Fig. 1*E*). Lung sections were also stained with Masson's trichrome to evaluate fibrosis, and stained with α-smooth muscle actin. Sizes of both the peribronchial smooth muscle area and lung fibrosis area were increased in OVA-sensitized control mice; however, mice administered rAg85B showed strong suppression of both fibrosis and α-smooth muscle actin expression as well as reduction in inflammation severity assessed by H&E staining (Fig. 1*E*). These observations indicated that rAg85B has a critical function of regulating airway inflammation in a mouse model of allergen-induced asthma. Moreover, rAg85B i.n. administration induced wound repair including suppression of both fibrosis and α-smooth

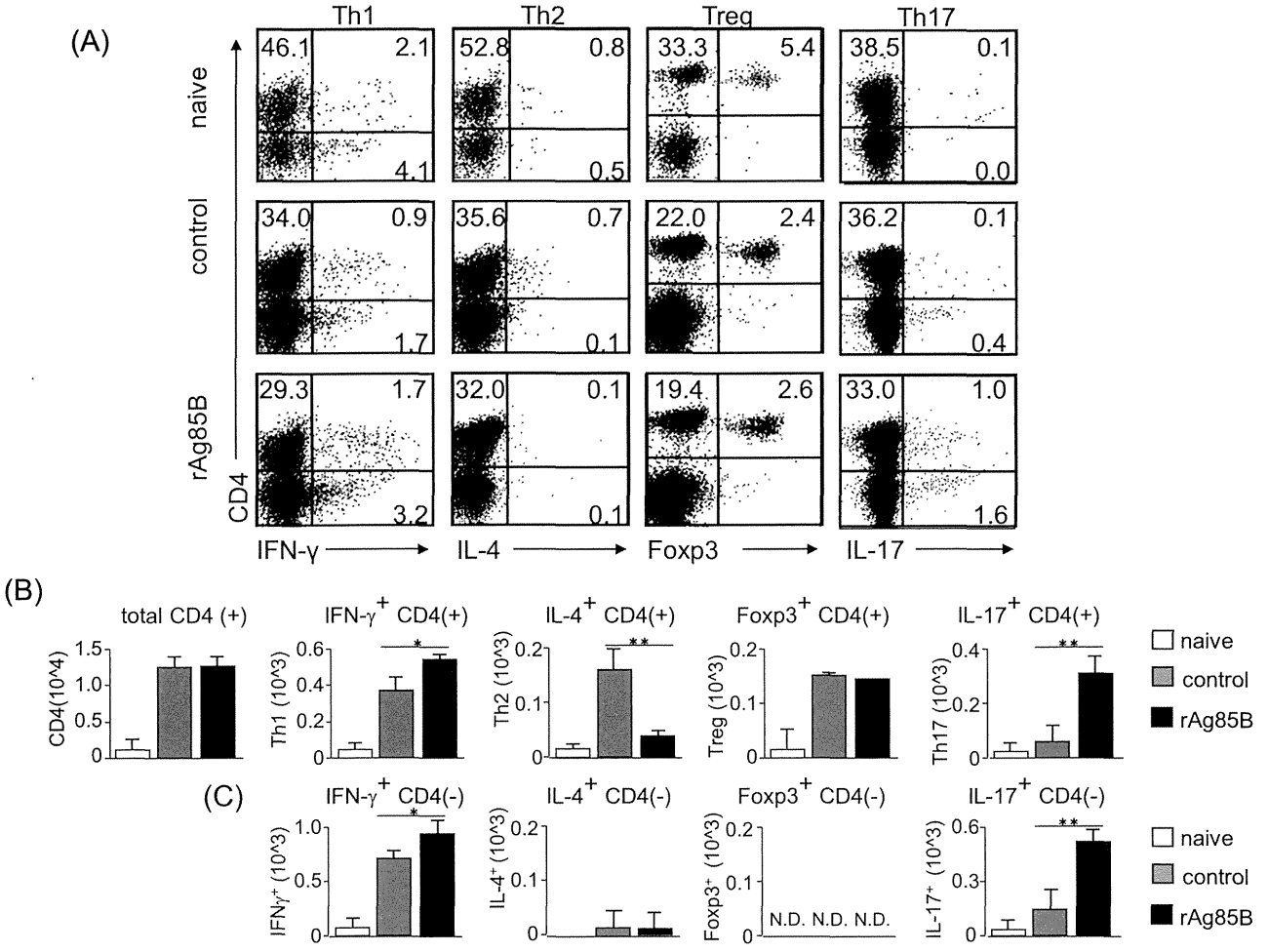

Figure 3. IFN-γ and IL-17-producing CD4 T cell subsets proliferated in lymph nodes after rAg85B administration. OVA-immunized (i.p., day0 and 14) and sensitized (5% aerosolized-OVA, day21 to 25) BALB/c mice were challenged with PBS or rAg85B protein (i.p. (100 μg; days 0 and 14) and i.n. (20 μg; days 21, 23, and 25)). At 24 h after the last OVA sensitization, mediastinal lymph nodes (MLNs) from naïve or OVA sensitized BALB/c mice treated with PBS or rAg85B, were harvested. MLNs were stimulated with ionomycin and PMA for 5 h, and with brefeldin A added in the last 3 h. Flow cytometry of stimulated MLNs from naïve (upper), PBS-treated (middle) and rAg85B protein-treated (lower) OVA-sensitized mice stained with specific antibodies indicated marker. Numbers in quadrants indicate percent of cells in each (*A*). Absolute numbers of various cell populations (above graphs) in lymph nodes (*B*, *C*). Data are representative of three independent experiments (*P<0.05, **P<0.01 compared with OVA control. error bars, s.d.; n = 6 mice).
doi:10.1371/journal.pone.0106807.g003

muscle actin expression. Incidentally, previous data showed that either i.p. (days 0, 14) or i.n. (days 21, 23, and 25) challenge with rAg85B did not induce strong suppression of Th2-response in OVA-sensitized mice (data not shown).

Immune deviation from a Th2-response towards a Th1, Th17-related response by rAg85B administration

We next assessed the production of OVA-specific cytokines in lymph node cells after *in vitro* stimulation with OVA (Fig. 2). Cells from mediastinal lymph nodes (mLNs) were stimulated *in vitro* with OVA and the production of various types of cytokines was assessed. The level of the Th1 cytokine IFN-γ in culture supernatants of cells from rAg85B-administered mice was increased. On the other hand, the levels of Th2 cytokines IL-5 and IL-13 in culture supernatants of cells from rAg85B-administered mice were lower than those in culture supernatants of cells from control mice. Similarly, mice administered rAg85B showed inhibition of production of the CCL5 (RANTES) and the thymus- and activation-regulated chemokine CCL17 (TARC), which contribute to allergic inflammation. Production of IL-17, IL-22 and TNF-α was also enhanced in culture supernatants of OVA-stimulated mLN cells from rAg85B-administered mice. These results suggested that Th1 and Th17 cytokines are crucial factors in the suppressive effect of rAg85B on airway inflammation.

$CD4^+$ T cells producing IFN-γ and IL-17 were increased in mediastinal lymph nodes by rAg85B administration

We next examined Th cell responses in the mouse asthma model by intracellular staining analysis. mLN cells were stimulated with or without PMA and ionomycin, and cell fractions were analyzed by intracellular cytokine staining. Stained $CD4^+$ T cells producing IFN-γ or IL-17 were increased in mice administered rAg85B, whereas IL-4-secreting cells were decreased in those mice (Fig. 3*A*, *3B*). On the other hand, rAg85B administration was not associated with the induction of Treg cells, which express Foxp3

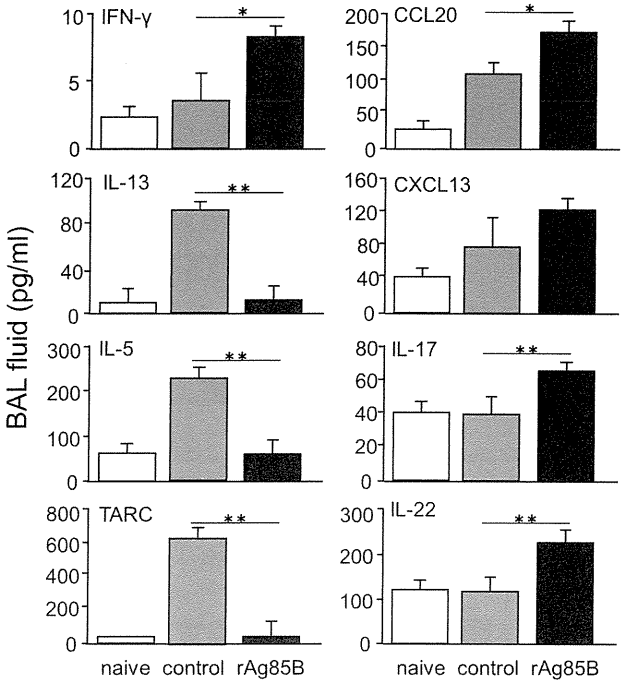

Figure 4. Administration of rAg85B resulted in the reduction of Th2 cytokine and chemokine levels and in the enhancement of Th1 and Th17 cytokine levels in BAL fluid. OVA-immunized (i.p., day0 and 14) and sensitized (5% aerosolized-OVA, day21 to 25) BALB/c mice were challenged with PBS or rAg85B protein (i.p. (100 μg; days 0 and 14) and i.n. (20 μg; days 21, 23, and 25)). At 24 h after the last OVA sensitization, BAL fluid from naïve or OVA sensitized BALB/c mice treated with PBS or rAg85B, were harvested. Levels of cytokines in the BAL fluid were measured directly by ELISA. Data are representative of at least three independent experiments (*P<0.05, **P<0.01 compared with OVA control. error bars, s.d.; n = 6 mice).
doi:10.1371/journal.pone.0106807.g004

and CD25, in LNs (Fig. 3*A*, *3B*, S2). These results were the same for not only the fraction of $CD4^+$ T cells but also the fraction of $CD4^-$ cells producing cytokines in mLNs (Fig. 3*C*). These results suggested that rAg85B administration was involved in the induction of IFN-γ or IL-17-producing $CD4^+$ T cells and $CD4^-$ cells in LNs.

Mice administered rAg85B showed reduction in levels of Th2 cytokines and chemokines levels and increase in levels of Th1 and Th17 cytokines in BAL

The pathogenesis of asthma is associated with many cell types and several molecular/cellular pathways in the lung. Therefore, we investigated whether rAg85B administration regulates various cytokines associated with the pathogenesis of allergic inflammation in BAL fluid. Control mice in which allergic inflammation developed showed increased production of Th2 cytokines and chemokines in BAL fluid, such as IL-13, IL-5 and TARC. Mice administered rAg85B showed inhibition of the induction of IL-13, IL-5 and TARC (Fig. 4). Furthermore, enhancement of IFN-γ, IL-17 and IL-22 production was observed in BAL fluid from mice administered rAg85B. Production of chemokines secreted from non-T cells, CCL20 and CXCL13, was also increased in BAL fluid from rAg85B-administered mice. The chemokine CCL20 is thought to be associated with the recruitment of Th17 lymphocytes and LTi-like or NK-like cells [17,18], and CXCL13 is a chemokine ligand of C-X-C motif receptor 5 (CXCR5) that is expressed on Lti-like cells. These findings suggested that rAg85B administration was involved in induction of immune responses from both $CD4^+$ T cells and other innate cells in BAL fluid of mice in which allergic inflammation has developed.

rAg85B administration elicits IL-17-producing CD4-negative cells rather than $CD4^+$ T cell subsets in BAL fluid

To determine the peripheral Th cell population in the lungs of rAg85B-treated mice, BAL cells from experimental mice were analyzed by intracellular cytokine staining. The percentages of IFN-γ and IL-17-positive cells from rAg85B-administered mice were higher than those from control cells in agreement with the results of FACS analysis of mLN cells (Fig. 5*A*), and Treg cells in BAL fluid from rAg85B-administered mice were also the same as the results for mLN cells (Fig. 5*A*). The absolute number of $CD4^+$ T cells stained for IL-17 was not increased in BAL cells from rAg85B-administered mice, unlike the results for mLN cells; however, total IL-17-secreting cells, $CD4^-$ $IL\text{-}17^+$ cells, were increased in rAg85B-administered mice compared with those in control mice (Fig. 5*B*, *5C*). $CD4^-$ IFN-γ-producing cells were observed in BAL fluid from rAg85B-administered mice as same to $CD4^+$ cells. In addition, IL-4-secreting $CD4^+$ cells were decreased in rAg85B-treated mice, whereas IL-4-producing $CD4^-$ cells were not observed. These observations indicated that IL-17 was produced by $CD4^-$ cells rather than by $CD4^+$ T cells in BAL, unlike IFN-γ and IL-4. Furthermore, the types of BAL cells greatly changed after rAg85B treatment (Figure S3).

rAg85B administration was involved in recruitment of innate immune cells that secrete IL-17-related cytokines in BAL fluid

Recent studies have demonstrated that IL-17 was not only secreted by Th17 cells and the source of Th17-related cytokines was modified in various environmental conditions [19]. Mice administered rAg85B showed infiltration of CD4-negative immune cells, which secreted IL-17 cytokine in BAL fluid (Fig. 4, Fig. 5). From these findings, we next investigated the proportions of infiltrating $CD4^-$ cells that produce IL-17, including γδT cells, $IL\text{-}7R^+$ Lin^- cells (LTi-like cells), $CD3^-$ $NKp46^+$ cells and $CD11c^+$ cells, in BAL fluid from experimental mice. OVA-sensitized BALB/c mice administered rAg85B, but not mice administered PBS, showed an increased number of innate immune cells in BAL fluid (Fig. 6*A*). The percentages of $CD4^+$ and $CD8^+$ T cells in BAL fluid from rAg85B-administered mice were similar to those in BAL fluid from control mice. However, the percentages of γδT cells, LTi-like cells, $NKp46^+$ cells, and $CD11c^+$ cells in BAL fluid from rAg85B-administered mice were higher than those in BAL fluid from control mice (Fig. 6*A*). Since innate immune cells, which secrete IL-17 and related cytokines, IL-22, were thought to be induced by rAg85B administration, we next explored the source of IL-17-related cytokines in BAL fluid. Small numbers of IL-17-producing γδT cells, LTi-like cells and $CD11c^+$ cells were observed (Fig. 6*D*, *6F*, *6G*), while production of IL-17 from CD8+ T cells and $NKp46^+$ cells was not detected (Fig. 6*C*, *6E*). In the present study, a Th17-related cytokine, IL-22, was also detected in BAL fluid from mice administered rAg85B. (Fig. 4). All of the cells from BAL secreting Th17-related cytokines, including $CD4^+$ T cells, γδT cells, $NKp46^+$ cells, LTi-like cells and $CD11c^+$ cells, that were examined in this study showed IL-22 production in mice administered rAg85B (Fig. 6*B*, *6D*, *6E*, *6F*, *6G*). On the other hand, production of IL-17 from $NKp46^+$ cells and $CD11c^+$ cells were not detected (Fig. 6*E*, *6G*). Although it is now known that NKT cells, alveolar macrophages and neutrophils might also

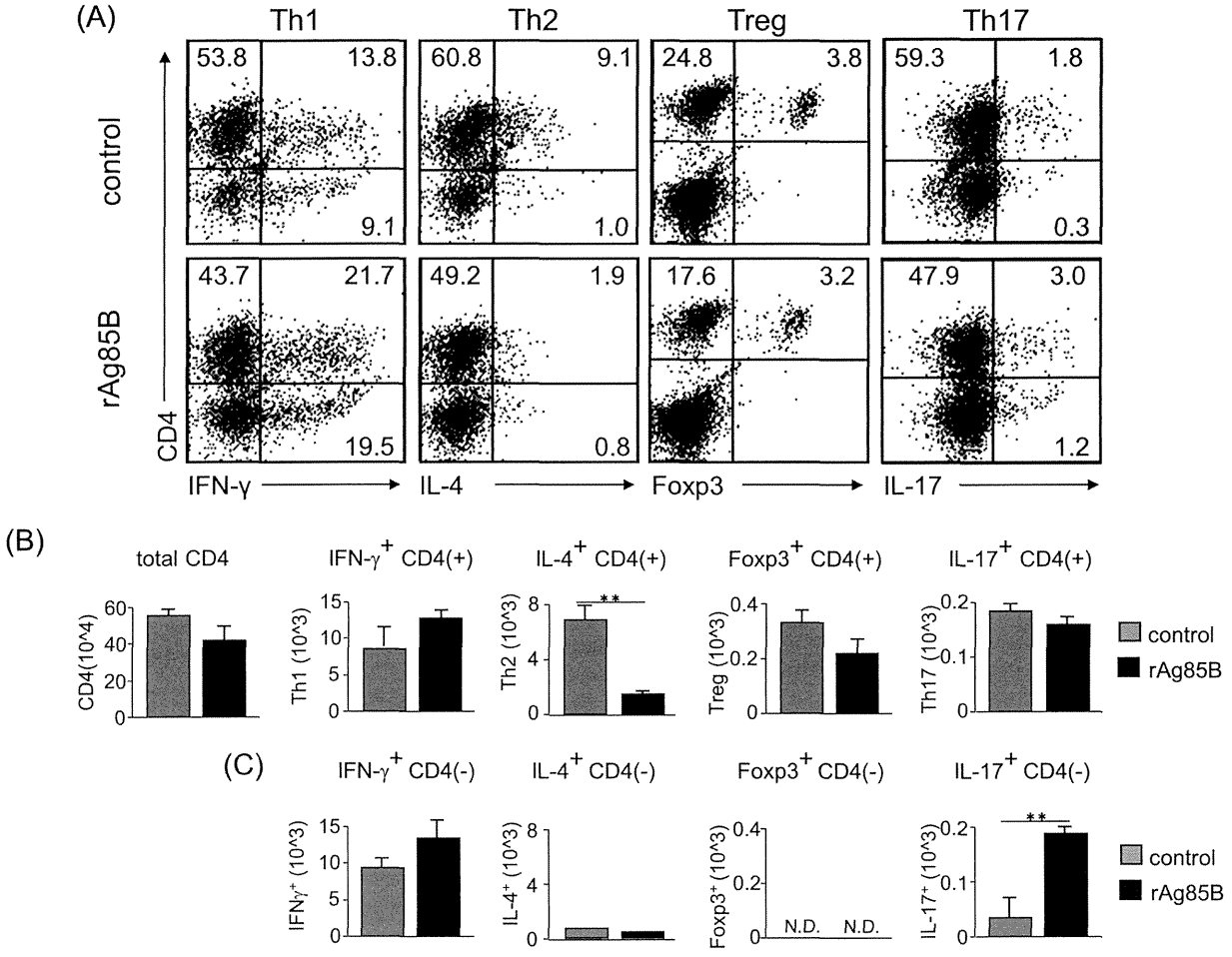

Figure 5. IFN-γ and IL-17-producing CD4-negative cell subsets proliferated in BAL fluid after rAg85B administration. OVA-immunized (i.p., day0 and 14) and sensitized (5% aerosolized-OVA, day21 to 25) BALB/c mice were challenged with PBS or rAg85B protein (i.p. (100 μg; days 0 and 14) and i.n. (20 μg; days 21, 23, and 25)). At 24 h after the last OVA sensitization, BAL fluid from naïve or OVA sensitized BALB/c mice treated with PBS or rAg85B, were harvested. BAL cells were stimulated with ionomycin and PMA for 5 h, and with brefeldin A added in the last 3 h. Flow cytometry of stimulated BAL cells from PBS-treated (upper) and rAg85B protein-treated (lower) OVA-sensitized mice stained with specific antibodies indicated marker. Numbers in quadrants indicate percent of cells in each (*A*). Absolute numbers of various cell populations (above graphs) in BAL fluid (*B*, *C*). Data are representative of three independent experiments (**P<0.01 compared with OVA control. error bars, s.d.; n = 6 mice).
doi:10.1371/journal.pone.0106807.g005

produce IL-17 in certain conditions, the numbers of these IL-17-secreting cells in BAL fluid from rAg85B-administered mice showed little or no change compared with those in the control group in our experimental setting. Remarkably, these responses induced by rAg85B were observed in allergic animals but not in naïve ones (data not shown).

Functions of IL-17 and IL-22 in rAg85B-administered mice

We next investigated the importance of Th17-related cytokines by using neutralizing antibodies (Abs) to IL-17 and IL-22 in rAg85B-administered experimental mice. Administration of neutralizing Abs to IL-17 and IL-22 did not show any systemic inhibitory effects induced by rAg85B as a result of IgE production (Fig. 7*A*). Furthermore, neutralization of IL-17 and IL-22 did not restore the functions of rAg85B with immune deviation from a disease-promoting Th2 response towards a Th1 response, whereas inhibition of TARC production regulated by rAg85B was reversed by neutralizing IL-22 Abs treatment (Fig. 7*B*). These results suggested that IL-17 and IL-22 induced by rAg85B have little or no systemic inhibitory effect on the development of allergic inflammation in the lung. Neutralization of IFN-γ at the challenge phase also had little or no suppressive effect on serum IgE expressions and eosinophilia induced by rAg85B treatment. (data not shown). The number of infiltrating cells in BAL fluid were also not changed in mice administered neutralizing Abs to IL-17 and IL-22 (Fig. 7*C*); however, fractions of infiltrating cells in BAL fluid were different. Neutralization of IL-17 by IL-17-specific Abs prevented neutrophil infiltration by rAg85B administration in the airway, and this preventive effect on infiltration of neutrophils was partial in IL-22-specific Abs administered mice (Fig. 7*D*). Eosinophilia suppression by rAg85B administration was reversed by neutralizing IL-22 Abs treatment (Fig. 7*D*). These results parallel previous observations of the specificity of IL-17 and IL-22 effects [20]. Enhancement of innate immune cell recruitment induced by rAg85B was fully reversed by neutralizing IL-17 Abs treatment, and this rAg85B effect was partially reversed by administration of neutralizing IL-22 Abs in γδT cells (Fig. 7*D*). These results showed that Th17-related cytokines induced by rAg85B have pivotal roles in innate immune cell recruitment in BAL fluid and in severity of

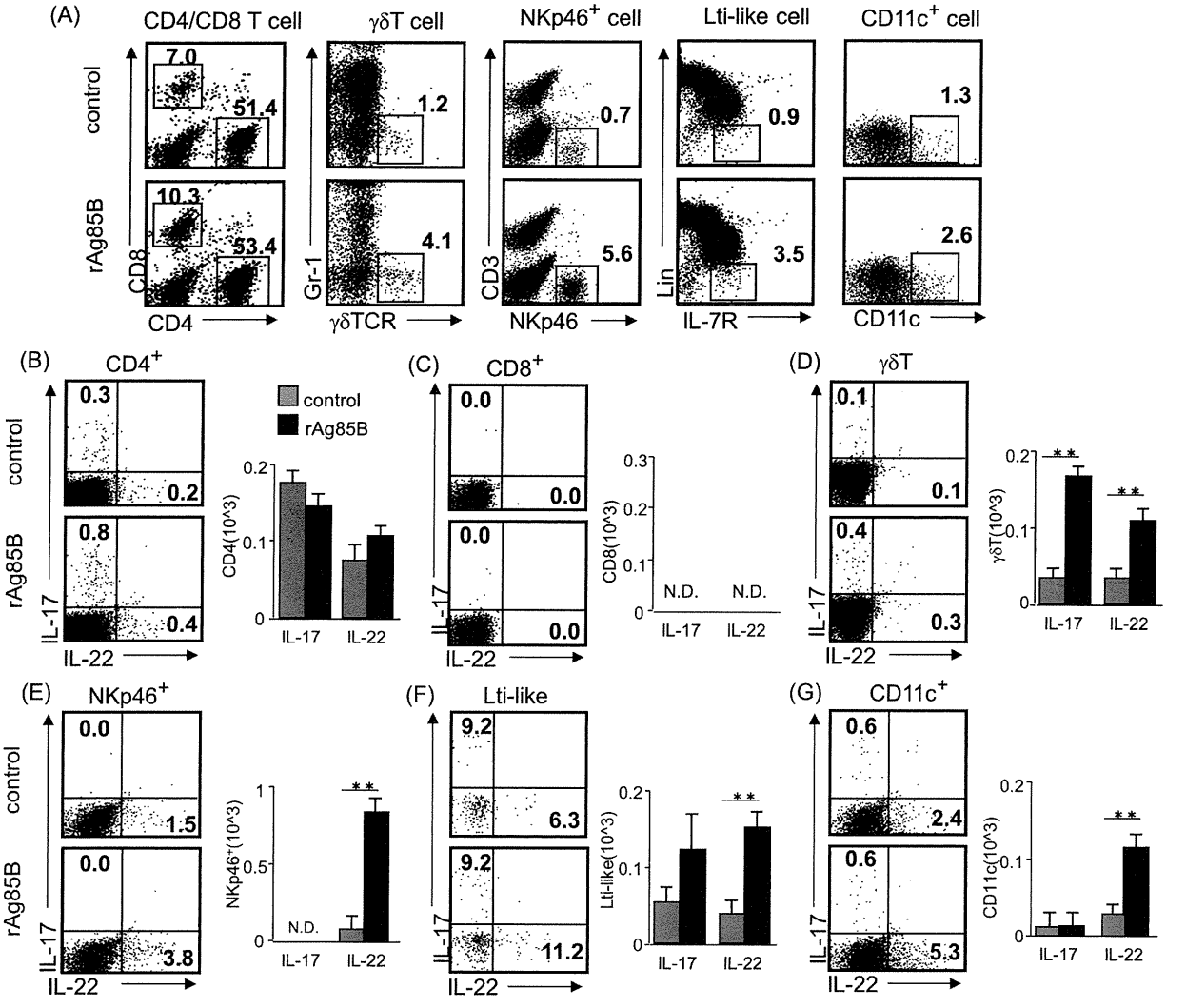

Figure 6. Innate immune cells that secrete Th17-related cytokines are induced by rAg85B administration in BAL fluid. OVA-immunized (i.p., day0 and 14) and sensitized (5% aerosolized-OVA, day21 to 25) BALB/c mice were challenged with PBS or rAg85B protein (i.p. (100 μg; days 0 and 14) and i.n. (20 μg; days 21, 23, and 25)). At 24 h after the last OVA sensitization, BAL fluid from naïve or OVA sensitized BALB/c mice treated with PBS or rAg85B, were harvested. BAL cells were stimulated with ionomycin and PMA for 5 h, and with brefeldin A added in the last 3 h. Flow cytometry of BAL cells from PBS-treated (upper) and rAg85B protein-treated (lower) OVA-sensitized mice stained with anti-CD3, anti-CD4, anti-CD8, anti-Gr-1, anti-γδ TCR, anti-NKp46, anti-CD11c, anti-CD127 (IL-7R) and Lineage specific marker (CD3, CD19, Gr-1, CD11b, CD11c). Numbers in quadrants indicate percent of cells in each (*A*). Intracellular IL-17 and IL-22 staining in indicated cells by flow cytometry (dot plots) and absolute numbers of those cell populations (side graphs) in the BAL fluid (*B, C, D, E, F, G*). Data are representative of at least two independent experiments (**P<0.01 compared with OVA control. error bars, s.d.; n = 6 mice).
doi:10.1371/journal.pone.0106807.g006

lung inflammation but not in regulated systemic allergic inflammation involving Th responses.

Administration of rAg85B promoted Th17-related innate responses in the lung

Our data suggested an important link between rAg85B and airway innate immune cells producing IL-17 and IL-22 that contributed to the homeostasis expression of Th17-related cytokine response genes. However, these two cytokines induced by rAg85B administration did not clearly show inhibitory effects on systemic allergy responses (Fig. 7*A*, 7*B*). From these findings, we next explored the relationship between the roles of airway innate immune cells and wound repair in mice that received i.n. administration of rAg85B. Mice that received IL-17 or IL-22 or both neutralizing antibodies showed a marked induction of fibrosis and actin staining but incomplete cancellation of rAg85B suppressive effects at the same levels as those in OVA control mice (Fig. 8*A*). Histological findings suggested that IL-17 and IL-22 induced by rAg85B i.n. administration were partially involved in regulation of local tissue allergic inflammation. The inhibition of rAg85B effects by neutralizing Abs of IL-17 and IL-22 to allergic inflammation was partial; however, tissue repair in lungs was seen in rAg85B-administered mice by histopathological examination. These results led us to hypothesize that IL-17 and IL-22 induced by rAg85B induced local tissue remodeling/repair molecules. To confirm this, the induction of tissue homeostasis-related gene expression in rAg85B-administered mice was examined by real-time RT-PCR. Rb2, Cyclin D1 and c-Myc are associated with

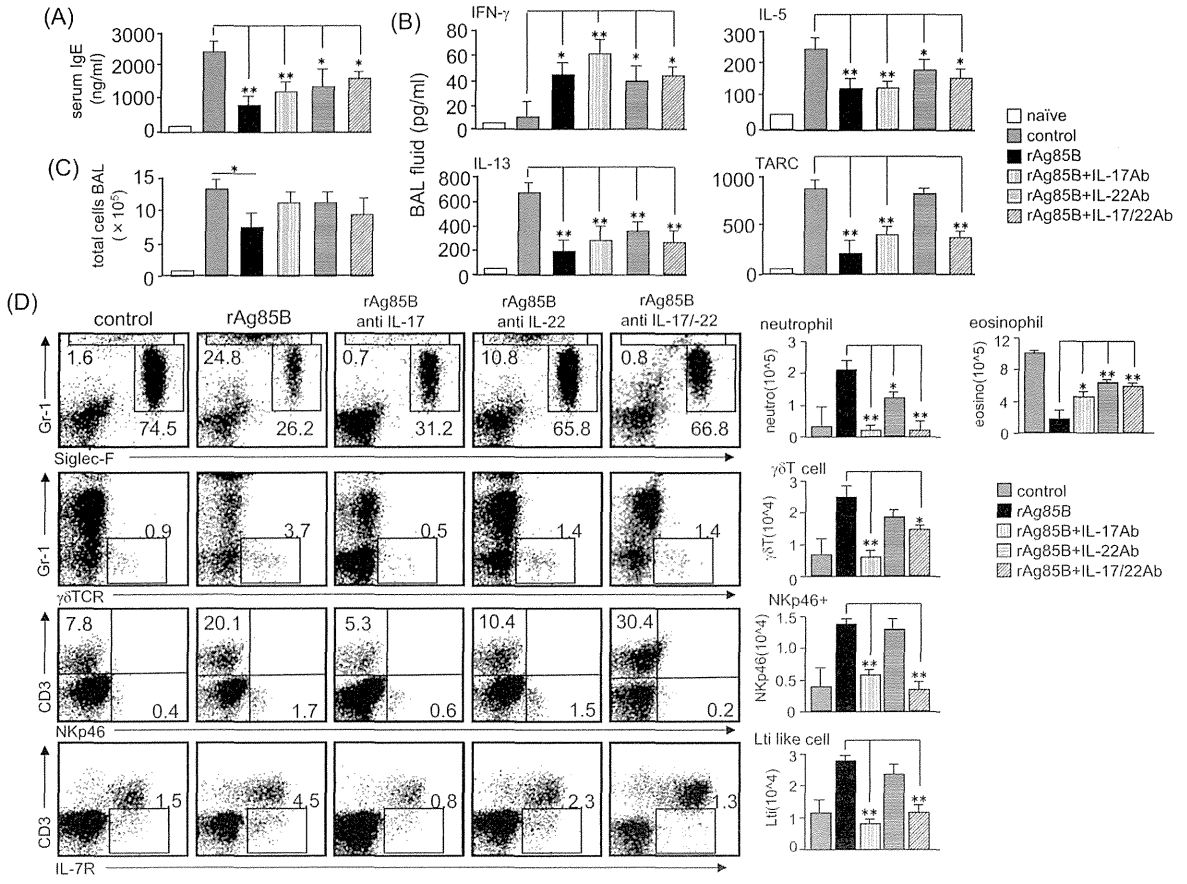

Figure 7. Neutralization of Th17-related cytokines inhibits cell recruitment to the lung but does not change cytokine and chemokine production. OVA-sensitized BALB/c mice (5% aerosolized-OVA, day21 to 25) were challenged intranasally with PBS (control), rAg85B (rAg85B + isotype-matched control antibody (Ab)), rAg85B plus neutralizing IL-17 (rAg85B + IL-17Ab) or IL-22 (rAg85B + IL-22Ab), or a combination of both antibodies (rAg85B +IL-17/22Ab) on days 21, 23, and 25. The isotype control was treated with the same time course as neutralization Ab i.n. administration. One day after the last challenge, OVA-specific serum IgE concentration and levels of cytokines and chemokines in BAL fluid were determined by ELISA (*A*, *B*). BAL cells from naïve or OVA sensitized BALB/c mice treated with PBS or rAg85B with/without neutralization Ab were counted (*C*), and were stained with anti-Gr-1, anti-Siglec-F, anti-gd TCR, anti-CD3, anti-NKp46, and anti-CD127 for flow cytometric analysis. Numbers adjacent to outlined area indicate percent of eosinophils (Gr-1^{dull}, Siglec-F^{+}), neutrophils (Gr-1^{+}, Siglec-F^{neg}), γδT cells (Gr-1^{neg}, γδTCR^{+}), NKp46^{+} cells (CD3^{neg}, NKp46^{+}), LTi like cells (CD3^{neg}, L-7R^{+}), and absolute numbers of those cell populations (side graphs) in BAL fluid (*D*). Data are representative of at least two independent experiments (*P<0.05, **P<0.01 compared with rAg85B+isotype control challenged group. error bars, s.d.; n = 6 mice).
doi:10.1371/journal.pone.0106807.g007

wound healing, tissue repair and remodeling including proliferative molecules [21]. Muc1 [22,23], matrix metalloproteinase 13 (MMP13) [24], and the extracellular matrix proteins decorin and dermatopontin [25] produce protective mucus. Lymphotoxin-beta (Ltb) is a molecule related to signaling in stromal cells to produce factors that organize lymphoid cells into lymph nodes [26]. The transcription of Reg3γ is involved in tissue repair and antimicrobial responses [27]. The expression of these genes involved in innate immune response-mediated signaling was significantly enhanced in the lungs of rAg85B-administered mice (Fig. 8*B*). The increases in mRNA levels of all molecules other than Reg3γ and dermatopontin were inhibited by treatment with neutralizing Abs of IL-17 (Fig. 8*B*). On the other hand, the expression of mRNA of molecules enhanced by rAg85B administration was decreased after treatment with IL-22 neutralizing Abs except for Rb2, Cyclin D1, c-Myc, Mmp13 and Muc1 (Fig. 8*B*). These results suggested that IL-17 and IL-22 induced by rAg85B administration affected induction of pulmonary innate response. In conclusion, IL-17 induced by rAg85B administration induced the expression of various types of wound healing, tissue repair and remodeling molecules. Interestingly, IL-22 in rAg85B-immunized mice induces the expression of molecules mainly associated antimicrobial responses such as Reg3γ, decorin, dermatopontin and Ltb. In summary, Th1 and Th17 cells are induced in regional lymph nodes by administration of rAg85B; however, Th17 cells are not induced in BAL unlike in Th1 cells. IL-17 is produced by innate immune cells with IL-22 production. IL-17 and IL-22 are important in not only anti-allergic effects, such as eosinophil inhibition, but also wound healing and tissue repair in the lung (Fig. 9).

Discussion

Results of several experimental studies on mycobacteria involving mycobacterial antigens in mouse models of allergic airway inflammation have been reported. In murine asthma models, intranasal administration of BCG suppressed asthma manifestations probably through Th1 response [2,4], Treg cells [5,6,28], or NKT cells [7,8,29]. In our experimental setting using rAg85B protein, we did not find any detectable effect or

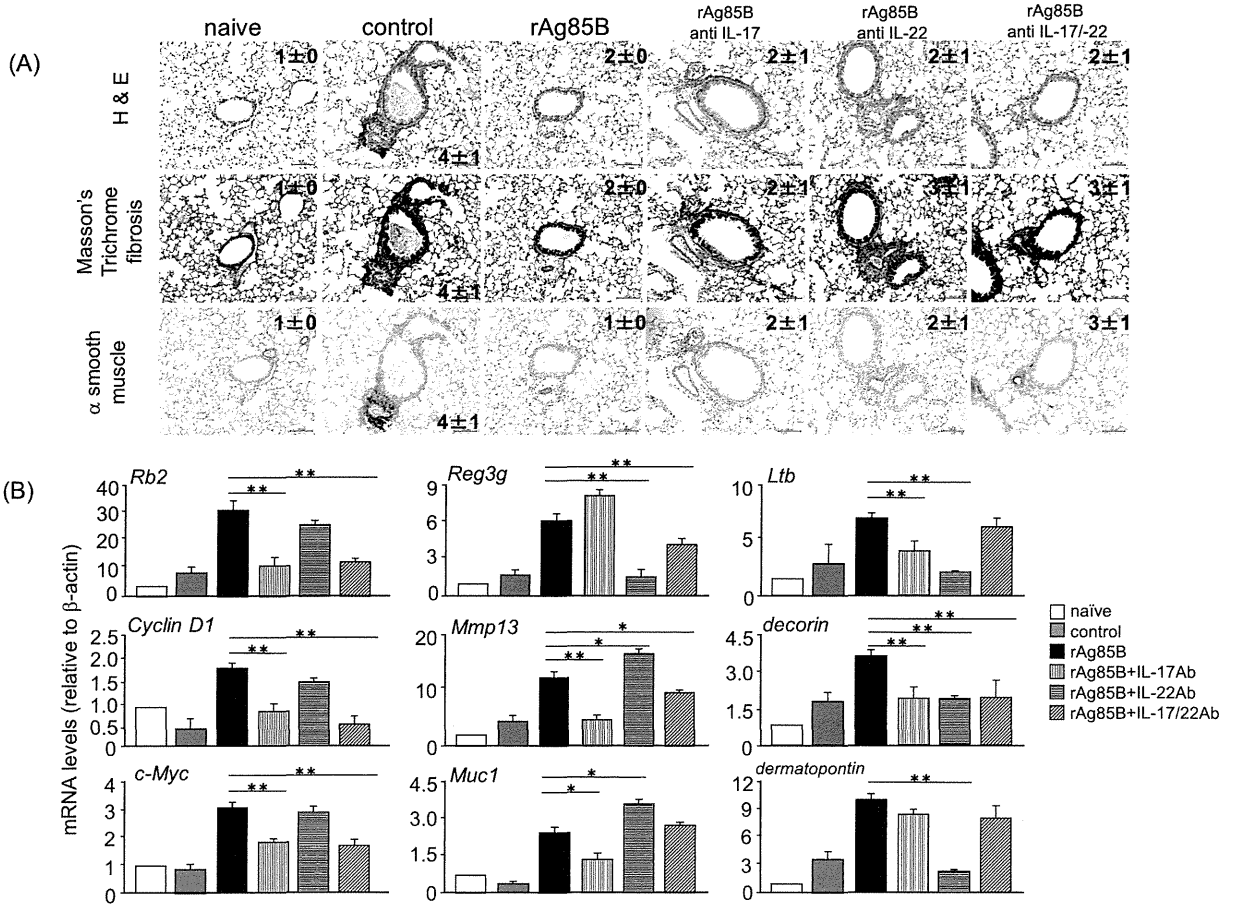

Figure 8. Ag85B administration promotes Th17-related innate responses in the lung. OVA-sensitized BALB/c mice (5% aerosolized-OVA, day21 to 25) were challenged intranasally with PBS (control), rAg85B (rAg85B + isotype control), rAg85B plus neutralizing IL-17 (rAg85B + IL-17Ab) or IL-22 (rAg85B + IL-22Ab), or a combination of both antibodies (rAg85B +IL-17/22Ab) on days 21, 23, and 25. The isotype-matched control antibody was treated with the same time course as neutralization Ab i.n. administration. Lungs from naïve or OVA sensitized BALB/c mice treated with PBS or rAg85B with/without neutralization Ab were sampled one day after the last challenge for histological analysis and quantification of mRNA levels. Lung sections were stained with hematoxylin and eosin (left row, scale bar, 100 mm), Masson's trichrome (center row, scale bar, 100 mm), α-smooth muscle actin (right row, scale bar, 50 mm). Numbers in quadrants indicate the score scale from 0 to 5 in each (*A*). Real-time RT-PCR was performed for the indicated molecules expression on RNA isolated from individual mice lungs (*B*). Data are representative of at least two independent experiments (*P<0.05, **P<0.01 compared with rAg85B+isotype control challenged group. error bars, s.d.; n = 6 mice).
doi:10.1371/journal.pone.0106807.g008

substantial change in numbers of both NKT cells and Treg cells in BAL fluid from rAg85B-administered mice. Moreover, microarray analysis revealed that the gene expression pattern of splenocytes stimulated with rAg85B and that of splenocytes stimulated with BCG were very different (data not shown). This discrepancy in the effects of vaccination with BCG and vaccination with rAg85B might be related to the factors affecting immune responses. BCG contains many essential components to induce early immune response such as glycolipid and DNA, whereas rAg85B is a single immunogenic protein.

The present study indicated that Th17-related immune responses induced by rAg85B administration had a suppressive effect on allergic airway inflammation, and we attributed this suppressive effect to the larger proportion of Th17-related cytokine-producing innate immune cells in BAL fluid. It has been reported that Mycobacterium antigens increased the number of γδT cells that express IFN-γ [30] or IL-17 [31], and these responses induce healing to epithelial surfaces [32]. Given the integral role of γδT cells in innate immunity, γδT cells are one of the crucial factors in the rAg85B immune regulatory functions. Interestingly, our study also showed that IL-22-producing cells in lungs of rAg85B-administered mice were $NKp46^+$ cells, LTi-like cells, γδT cells and $CD11c^+$ cells. This is the first time demonstration of an important link between the mycobacterium antigen rAg85B and IL-22-producing cells. Although we could not rule out the possibility of Th17 cytokine-producing cells other than those described here, $NKp46^+$ cells, LTi-like cells, γδT cells and $CD11c^+$ cells were thought to be rapid innate sources of IL-22, which is required in the early stage to maintain epithelial cell integrity and to suppress eosinophilia. Moreover, IL-22 can act synergistically or additively with other cytokines, including IL-17 or TNF, to promote gene expression for antimicrobial peptides, chemokines, matrix metalloproteinases, cytokines, and acute-phase proteins from epithelial cells in the lung [33]. These findings also support our results showing that simultaneous induction of these cytokines and expression of many genes may be beneficial functions of rAg85B treatment in local allergic pathology.

Pulmonary infection of mycobacteria induced not only a neutrophil-mediated response but also T cell-mediated IFN-γ

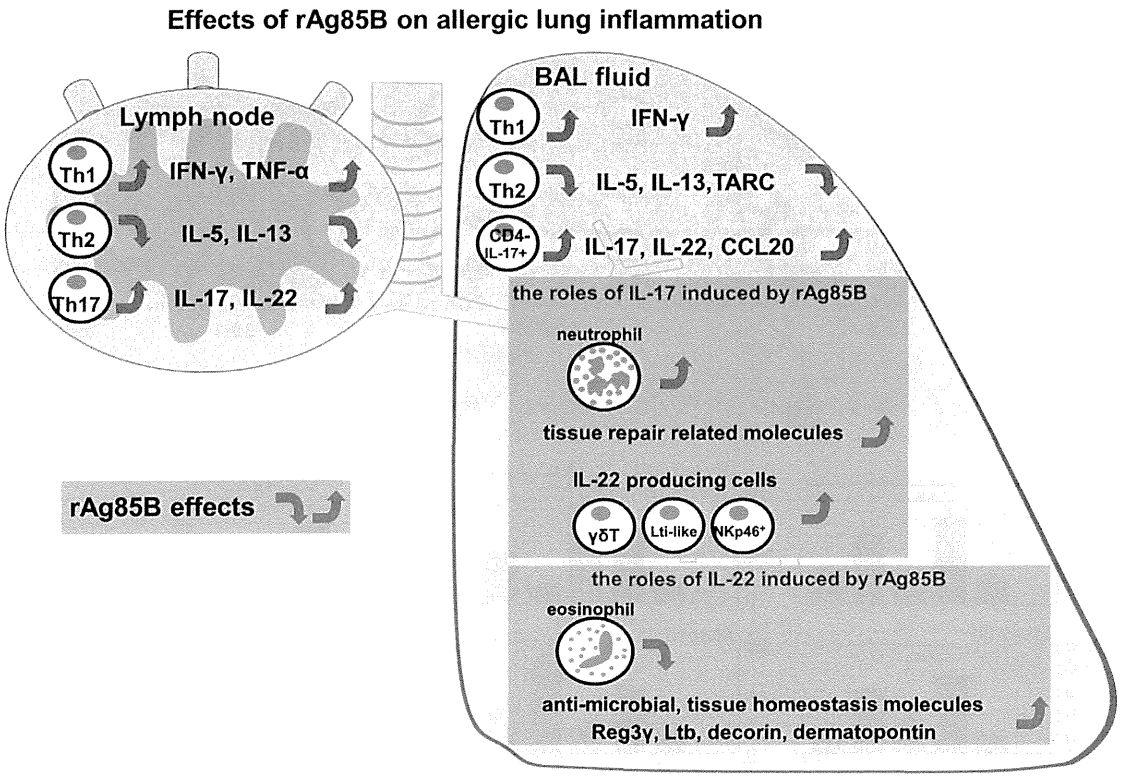

Figure 9. Schematic illustration of the proposed effects of rAg85B in a mouse model of allergic inflammation. IFN-γ and IL-17-producing Th cells are induced in regional lymph nodes by rAg85B challenge, however, Th17 cells do not enter the lung unlike Th1 cells. Th17-related cytokine-secreting cells in lungs from rAg85B-administered mice are innate immune cells including γδT cells, IL-7R$^+$ Lin$^-$ cells, CD3$^-$ NKp46$^+$ cells and CD11c$^+$ cells. IL-17 and IL-22 induced by rAg85B in an allergic environment have crucial roles in not only anti-allergic effects but also regulation of tissue homeostatic reactions.
doi:10.1371/journal.pone.0106807.g009

production and granuloma formation depending on IL-17 from especially γδT cells [34]. The hallmark of mycobacterial infection in the lung is granuloma formation with infiltrating neutrophils, which creates an immune microenvironment in which the infection can be controlled. On the other hand, it also provides the mycobacterium with a niche in which it can survive, modulating the immune response to ensure its survival without damage over a long period of time [35,36]. Mature granulomas include fibroblasts and extracellular matrix, which surround and separate the granulomas from the normal environment. Administration of anti-IL-17 Abs during the inhalatory challenge phase abolished the bronchial neutrophilia and the upregulation of genes related to tissue repair and homeostasis observed in rAg85B-administered mice in the present study. Neutrophils may also promote epithelial healing [37] and are now known to be rich sources of prestored and expressible proteins [38] that may directly promote wound healing [39,40]. In the present study, induction of neutrophilia and upregulation of described genes related to wound healing with suppression of tissue injury might be the mechanisms of granuloma formulation induced by mycobacteria infection.

In the present study, IFN-γ and Th17-related cytokines were key factors to regulate allergic severity in our experimental setting. Although infiltration of Th1 and Th17 cells elicited by rAg85B was induced in pulmonary lymph nodes, such effector cells were not increased in BAL fluid of mice showing anti-allergic effects of Ag85B administration. Moreover, our results suggested that the accumulation of neutrophils and IL-17 and/or IL-22-producing innate immune cells contributed to the homeostatic functions in the Th1-balanced environment induced by rAg85B administration. These findings provide a new insight into the regulatory effects of various innate immune factors induced by the mycobacteria major secretion protein rAg85B in allergic inflammation.

Supporting Information

Figure S1 SDS-PAGE separation and silver staining of rAg85B. The recombinant purified Ag85B was solubilized in sample buffer to the desired concentration, and boiled for 5 min. 15 μl/well from each samples were separated on 10% SDS gel using mini-PROTEAN electrophoresis instrument (Bio-Rad Laboratories). Silver staining of the gel was performed according to the standard protocol of EzStain Silver (ATTO). Various concentration of rAg85B on the gel (12.5, 25, 50, 100, 200, and 400 ng).
(TIF)

Figure S2 CD4$^+$ Foxp3$^+$ T cells were almost expressing CD25. OVA-immunized (i.p., day0 and 14) and sensitized (5% aerosolized-OVA, day21 to 25) BALB/c mice were challenged with PBS or rAg85B protein (i.p. (100 μg; days 0 and 14) and i.n. (20 μg; days 21, 23, and 25)). At 24 h after the last OVA sensitization, mediastinal lymph nodes (MLNs) from naïve or OVA sensitized BALB/c mice treated with PBS or rAg85B, were harvested. MLNs cells from naïve (upper), PBS-treated (middle) and rAg85B protein-treated (lower) OVA-sensitized mice were

stained with anti-CD4 and anti-Foxp3. Cells in R1-R4 were analyzed for the expression of CD25.
(TIF)

Figure S3 The composition of BAL cells in rAg85B administered mice. OVA-immunized (i.p., day0 and 14) and sensitized (5% aerosolized-OVA, day21 to 25) BALB/c mice were challenged with PBS (control) or rAg85B (i.p. (100 μg; days 0 and 14) and i.n. (20 μg; days 21, 23, and 25)). One day after the last challenge, BAL cells from OVA sensitized BALB/c mice treated with PBS or rAg85B were counted. Different BAL cells populations were measured by surface staining. Flow cytometry of BAL cells stained with anti-CD3, anti-CD4, anti-CD8, anti-Gr-1, anti-γδ TCR, anti-NKp46, anti-CD11c, anti-CD127 (IL-7R) and Lineage specific marker (CD3, CD19, Gr-1, CD11b, CD11c).
(TIF)

Author Contributions

Conceived and designed the experiments: YY. Performed the experiments: YT HI MY. Analyzed the data: YY KM. Contributed reagents/materials/analysis tools: TF. Contributed to the writing of the manuscript: YT YY.

References

1. Adams JF, Scholvinck EH, Gie RP, Potter PC, Beyers N, et al. (1999) Decline in total serum IgE after treatment for tuberculosis. Lancet 353: 2030–2033.
2. Herz U, Gerhold K, Gruber C, Braun A, Wahn U, et al. (1998) BCG infection suppresses allergic sensitization and development of increased airway reactivity in an animal model. J Allergy Clin Immunol 102: 867–874.
3. Cavallo GP, Elia M, Giordano D, Baldi C, Cammarota R (2002) Decrease of specific and total IgE levels in allergic patients after BCG vaccination: preliminary report. Arch Otolaryngol Head Neck Surg 128: 1058–1060.
4. Choi IS, Koh YI (2002) Therapeutic effects of BCG vaccination in adult asthmatic patients: a randomized, controlled trial. Ann Allergy Asthma Immunol 88: 584–591.
5. Stassen M, Jonuleit H, Muller C, Klein M, Richter C, et al. (2004) Differential regulatory capacity of CD25+ T regulatory cells and preactivated CD25+ T regulatory cells on development, functional activation, and proliferation of Th2 cells. J Immunol 173: 267–274.
6. Robinson DS, Larche M, Durham SR (2004) Tregs and allergic disease. J Clin Invest 114: 1389–1397.
7. Cui J, Watanabe N, Kawano T, Yamashita M, Kamata T, et al. (1999) Inhibition of T helper cell type 2 cell differentiation and immunoglobulin E response by ligand-activated Valpha14 natural killer T cells. J Exp Med 190: 783–792.
8. Harada M, Magara-Koyanagi K, Watarai H, Nagata Y, Ishii Y, et al. (2006) IL-21-induced Bepsilon cell apoptosis mediated by natural killer T cells suppresses IgE responses. J Exp Med 203: 2929–2937.
9. Torrado E, Cooper AM (2010) IL-17 and Th17 cells in tuberculosis. Cytokine Growth Factor Rev 21: 455–462.
10. Griffiths KL, Pathan AA, Minassian AM, Sander CR, Beveridge NE, et al. (2011) Th1/Th17 cell induction and corresponding reduction in ATP consumption following vaccination with the novel Mycobacterium tuberculosis vaccine MVA85A. PLoS One 6: e23463.
11. Lambrecht BN, Hammad H (2012) The airway epithelium in asthma. Nat Med 18: 684–692.
12. Holgate ST (2012) Innate and adaptive immune responses in asthma. Nat Med 18: 673–683.
13. Sonnenberg GF, Fouser LA, Artis D (2011) Border patrol: regulation of immunity, inflammation and tissue homeostasis at barrier surfaces by IL-22. Nat Immunol 12: 383–390.
14. Takamura S, Matsuo K, Takebe Y, Yasutomi Y (2005) Ag85B of mycobacteria elicits effective CTL responses through activation of robust Th1 immunity as a novel adjuvant in DNA vaccine. J Immunol 175: 2541–2547.
15. Mori H, Yamanaka K, Matsuo K, Kurokawa I, Yasutomi Y, et al. (2009) Administration of Ag85B showed therapeutic effects to Th2-type cytokine-mediated acute phase atopic dermatitis by inducing regulatory T cells. Arch Dermatol Res 301: 151–157.
16. Karamatsu K, Matsuo K, Inada H, Tsujimura Y, Shiogama Y, et al. (2012) Single systemic administration of Ag85B of mycobacteria DNA inhibits allergic airway inflammation in a mouse model of asthma. J Asthma Allergy 5: 71–79.
17. Takatori H, Kanno Y, Watford WT, Tato CM, Weiss G, et al. (2009) Lymphoid tissue inducer-like cells are an innate source of IL-17 and IL-22. J Exp Med 206: 35–41.
18. Cella M, Fuchs A, Vermi W, Facchetti F, Otero K, et al. (2009) A human natural killer cell subset provides an innate source of IL-22 for mucosal immunity. Nature 457: 722–725.
19. Korn T, Bettelli E, Oukka M, Kuchroo VK (2009) IL-17 and Th17 Cells. Annu Rev Immunol 27: 485–517.
20. Schnyder B, Lima C, Schnyder-Candrian S (2010) Interleukin-22 is a negative regulator of the allergic response. Cytokine 50: 220–227.
21. Dieli F, Ivanyi J, Marsh P, Williams A, Naylor I, et al. (2003) Characterization of lung gamma delta T cells following intranasal infection with Mycobacterium bovis bacillus Calmette-Guerin. J Immunol 170: 463–469.
22. Sonnenberg GF, Nair MG, Kirn TJ, Zaph C, Fouser LA, et al. (2010) Pathological versus protective functions of IL-22 in airway inflammation are regulated by IL-17A. J Exp Med 207: 1293–1305.
23. Sugimoto K, Ogawa A, Mizoguchi E, Shimomura Y, Andoh A, et al. (2008) IL-22 ameliorates intestinal inflammation in a mouse model of ulcerative colitis. J Clin Invest 118: 534–544.
24. Planus E, Galiacy S, Matthay M, Laurent V, Gavrilovic J, et al. (1999) Role of collagenase in mediating in vitro alveolar epithelial wound repair. J Cell Sci 112 (Pt 2): 243–252.
25. Monticelli LA, Sonnenberg GF, Abt MC, Alenghat T, Ziegler CG, et al. (2011) Innate lymphoid cells promote lung-tissue homeostasis after infection with influenza virus. Nat Immunol 12: 1045–1054.
26. De Togni P, Goellner J, Ruddle NH, Streeter PR, Fick A, et al. (1994) Abnormal development of peripheral lymphoid organs in mice deficient in lymphotoxin. Science 264: 703–707.
27. Graf R, Schiesser M, Reding T, Appenzeller P, Sun LK, et al. (2006) Exocrine meets endocrine: pancreatic stone protein and regenerating protein–two sides of the same coin. J Surg Res 133: 113–120.
28. Zuany-Amorim C, Sawicka E, Manlius C, Le Moine A, Brunet LR, et al. (2002) Suppression of airway eosinophilia by killed Mycobacterium vaccae-induced allergen-specific regulatory T-cells. Nat Med 8: 625–629.
29. Taniguchi M, Harada M, Kojo S, Nakayama T, Wakao H (2003) The regulatory role of Valpha14 NKT cells in innate and acquired immune response. Annu Rev Immunol 21: 483–513.
30. Dieli F, Troye-Blomberg M, Ivanyi J, Fournie JJ, Bonneville M, et al. (2000) Vgamma9/Vdelta2 T lymphocytes reduce the viability of intracellular Mycobacterium tuberculosis. Eur J Immunol 30: 1512–1519.
31. Lockhart E, Green AM, Flynn JL (2006) IL-17 production is dominated by gammadelta T cells rather than CD4 T cells during Mycobacterium tuberculosis infection. J Immunol 177: 4662–4669.
32. Li Z, Burns AR, Miller SB, Smith CW (2011) CCL20, gammadelta T cells, and IL-22 in corneal epithelial healing. FASEB J 25: 2659–2668.
33. Guilloteau K, Paris I, Pedretti N, Boniface K, Juchaux F, et al. (2010) Skin Inflammation Induced by the Synergistic Action of IL-17A, IL-22, Oncostatin M, IL-1{alpha}, and TNF-{alpha} Recapitulates Some Features of Psoriasis. J Immunol.
34. Okamoto Yoshida Y, Umemura M, Yahagi A, O'Brien RL, Ikuta K, et al. (2010) Essential role of IL-17A in the formation of a mycobacterial infection-induced granuloma in the lung. J Immunol 184: 4414–4422.
35. Adams DO (1976) The granulomatous inflammatory response. A review. Am J Pathol 84: 164–192.
36. Sandor M, Weinstock JV, Wynn TA (2003) Granulomas in schistosome and mycobacterial infections: a model of local immune responses. Trends Immunol 24: 44–52.
37. Li Z, Burns AR, Han L, Rumbaut RE, Smith CW (2011) IL-17 and VEGF are necessary for efficient corneal nerve regeneration. Am J Pathol 178: 1106–1116.
38. Grenier A, Chollet-Martin S, Crestani B, Delarche C, El Benna J, et al. (2002) Presence of a mobilizable intracellular pool of hepatocyte growth factor in human polymorphonuclear neutrophils. Blood 99: 2997–3004.
39. Li Z, Rumbaut RE, Burns AR, Smith CW (2006) Platelet response to corneal abrasion is necessary for acute inflammation and efficient re-epithelialization. Invest Ophthalmol Vis Sci 47: 4794–4802.
40. Stirling DP, Liu S, Kubes P, Yong VW (2009) Depletion of Ly6G/Gr-1 leukocytes after spinal cord injury in mice alters wound healing and worsens neurological outcome. J Neurosci 29: 753–764.

Citation: Molecular Therapy—Nucleic Acids (2014) 3, e168; doi:10.1038/mtna.2014.20

www.nature.com/mtna

CD4+ T Cells Modified by the Endoribonuclease MazF Are Safe and Can Persist in SHIV-infected Rhesus Macaques

Naoki Saito[1], Hideto Chono[1], Hiroaki Shibata[2], Naohide Ageyama[2], Yasuhiro Yasutomi[2] and Junichi Mineno[1]

MazF, an endoribonuclease encoded by *Escherichia coli*, specifically cleaves the ACA (adenine–cytosine–adenine) sequence of single-stranded RNAs. Conditional expression of MazF under the control of the HIV-1 LTR promoter rendered CD4+ T cells resistant to HIV-1 replication without affecting cell growth. To investigate the safety, persistence and efficacy of MazF-modified CD4+ T cells in a nonhuman primate model *in vivo*, rhesus macaques were infected with a pathogenic simian/human immunodeficiency virus (SHIV) and transplanted with autologous MazF-modified CD4+ T cells. MazF-modified CD4+ T cells were clearly detected throughout the experimental period of more than 6 months. The CD4+ T cell count values increased in all four rhesus macaques. Moreover, the transplantation of the MazF-modified CD4+ T cells was not immunogenic, and did not elicit cellular or humoral immune responses. These data suggest that the autologous transplantation of MazF-modified CD4+ T cells in the presence of SHIV is effective, safe and not immunogenic, indicating that this is an attractive strategy for HIV-1 gene therapy.
Molecular Therapy—Nucleic Acids (2014) **3**, e168; doi:10.1038/mtna.2014.20; published online 10 June 2014
Subject Category: Therapeutic proof-of-concept Gene insertion, deletion & modification

Introduction

Antiretroviral therapy (ART), which is based on a combination of different classes of inhibitors, is widely used for the treatment of human immunodeficiency virus type 1 (HIV-1) infection and effectively suppresses HIV-1 replication to low or undetectable levels, corresponding with a recovery of CD4+ T cell counts.[1–3] ART treatment dramatically improves the survival rate of HIV-1-infected individuals and has transformed HIV-1 infection into a controllable illness. However, the need for lifelong therapy and difficulties in adherence to medication regimes are likely to lead to the emergence of drug-resistant HIV-1 strains. Long-term side effects, such as cardiovascular disease, hepatotoxicity and dementia, have been reported in association with HIV-1 infection.[4–6] The most serious deficiency of ART is that it cannot eradicate latent virus.[7] Once the treatment is interrupted, a replicable HIV-1 reemerges. Thus, the benefits of current ARTs are limited. Therefore, it remains necessary to discover and develop novel approaches for the management of HIV-1 infection, including treatment options used in combination with the ART.[8]

The report of the "Berlin Patient," who appears to have been cured of HIV-1 infection by stem cell transplantation with HIV-1 resistant CCR5Δ32/Δ32 cells[9] has had a major impact. This patient developed acute myelogenous leukemia and received bone marrow transplantation with cells bearing a homozygous Δ32 mutation in the CCR5 gene. No HIV-1 was detectable in this patient, even in the absence of ART.[10] However, allogeneic bone marrow transplantation as a cure for HIV-1 infection is not a realistic strategy because there is a risk of death, and the long-term effects are unclear. In contrast, gene therapy for HIV-1 has steadily progressed as an alternative to antiretroviral drug regimens.[11,12] A number of strategies have been developed, including strategies involving dominant negative inhibitory proteins, fusion inhibitors, antisense RNA, aptamers, RNA decoys, ribozymes, RNA interference, and HIV-1 entry inhibition.[13–18] These protocols target autologous T cells or hematopoietic stem cells for gene modification using retrovirus, lentivirus, or adenovirus vectors to deliver anti-HIV-1 payloads. Some of these methods have progressed to clinical trials.[19,20]

Recently, we proposed a new approach for gene therapy for HIV-1 using the endoribonuclease MazF.[21] MazF is encoded by *Escherichia coli* and specifically cleaves the ACA sequence of single-stranded RNAs. MazF does not interfere with ribosomal RNAs. When overexpressed in mammalian cells, MazF preferentially cleaves mRNA but not rRNA.[22] Previous studies have demonstrated that the expression of MazF under the control of the HIV-1 LTR promoter was successfully induced upon HIV-1 replication and rendered CD4+ T cells resistant to HIV-1 and simian/human immunodeficiency virus (SHIV) without affecting cellular mRNAs.[21,23] Because HIV-1 RNA has more than 240 ACA sequences, viral RNA is assumed to be highly susceptible to MazF. A key regulator of MazF expression in this system is the HIV-1 Tat protein, which activates transcription from the HIV-1 LTR.[24] In this system, the Tat protein induces HIV-1 replication and MazF expression. Furthermore, the autologous transplantation of MazF-modified CD4+ T cells in cynomolgus macaques has been shown to be safe, and the modified cells showed little or no immunogenicity.[25] These results suggest that the conditional expression of MazF is an attractive strategy for anti-HIV-1 gene therapy.

To investigate the safety, persistence and efficacy of MazF-modified CD4+ T cells in a nonhuman primate model *in vivo* in the presence of viral infection, six rhesus macaques were

[1]Center for Cell and Gene Therapy, Takara Bio Inc, Seta, Otsu, Shiga, Japan; [2]Tsukuba Primate Research Center, National Institute of Biomedical Innovation, Tsukuba, Ibaraki, Japan. Correspondence: Junichi Mineno, Center for Cell and Gene Therapy, Takara Bio Inc., Seta 3-4-1, Otsu, Shiga, 520–2193, Japan. E-mail: minenoj@takara-bio.co.jp or Hideto Chono, Center for Cell and Gene Therapy, Takara Bio Inc., Seta 3-4-1, Otsu, Shiga, 520–2193, Japan. E-mail: chonoh@takara-bio.co.jp

Keywords: gene therapy; HIV-1; MazF; primate model; rhesus macaque; retroviral vector; SHIV
Received 25 February 2014; accepted 27 April 2014; published online 10 June 2014. doi:10.1038/mtna.2014.20

infected with a SHIV 89.6P.[26] Four rhesus macaques were transplanted with MazF-modified CD4+ T (MazF-Tmac) cells, and two were transplanted with control ZsGreen1-modified CD4+ T (ZsG-Tmac) cells. After transplantation of the gene-modified cells, changes in the CD4+ T cell count values, changes in plasma SHIV viral loads, and the persistence of gene-modified cells were monitored throughout the experimental period. The humoral and cellular immune responses elicited by MazF were assessed. At necropsy, distributions of the transplanted MazF-Tmac cells in the distal lymphoid tissues, including several lymph nodes and the spleen, were analyzed.

Results

Study protocol and SHIV challenge

Six rhesus macaques (#12, #13, #14, #15, #16, and #17) were used for this experiment. Each rhesus macaque was challenged with SHIV 89.6P, followed by transplantation with autologous CD4+ T cells transduced with the MazF retroviral vector MT-MFR-PL2 (#12, #13, #14, and #15) or the control vector MT-ZGR-PL2 (#16 and #17) (Figure 1a). The rhesus macaques were monitored over 6 months for changes in CD4+ T cell counts, changes in SHIV viral loads in the plasma, persistence of the gene-modified cells, and the immune responses elicited by the gene-modified cells. An outline of the experiment is shown in Figure 1b,c. The dose of SHIV, day of infusion and experimental period are summarized in **Supplementary Table S1**. Initially, rhesus macaque #15 was challenged with (5000) 50% tissue culture infective dose ($TCID_{50}$), which we speculated would be a proper dose based on our previous experience; however, the viral loads declined to the limit of detection. We, therefore, increased the dose of $TCID_{50}$ for the other experiments. However, #12, #16, and #17 showed high viral loads, whereas #13 and #14 showed low viral loads. Such differences might have been due to individual variation in the sensitivity of the rhesus macaques used in this experiment.

Gene-modified T cell manufacturing and transplantation

MazF- or ZsGreen1-modified cells were manufactured from previously collected CD4+ T cells and transplanted into each rhesus macaque 2 months after SHIV 89.6P infection. Repeated transplantations were performed at 2-month intervals. To transplant more than 10^9 MazF-Tmac or ZsG-Tmac cells, $1–2\times10^7$ primary CD4+ T cells were recovered, stimulated, and transduced either with the MT-MFR-PL2 vector or the MT-ZGR-PL2 vector, and expanded as described in **Supplementary Materials and Methods**. The numbers and characteristics of the gene-modified CD4+ T cells for each transplantation are summarized in Table 1. The transduction efficiencies of the MazF and ZsGreen1 vectors were 52.0–69.5% and 53.8–75.7%, respectively. The gene-modified cells marked with a truncated form of the human low-affinity nerve growth factor receptor (LNGFR/CD271) were concentrated with an anti-CD271 monoclonal antibody for the first transplantation of rhesus macaques #12 and #14, and the second transplantation of rhesus macaques #13 and #15. The gene-modified cells that were positively selected were over 97% pure. There was no selection of control ZsG-Tmac cells for transplantation. The majority of the expanded cells were CD3+ CD4+ T cells

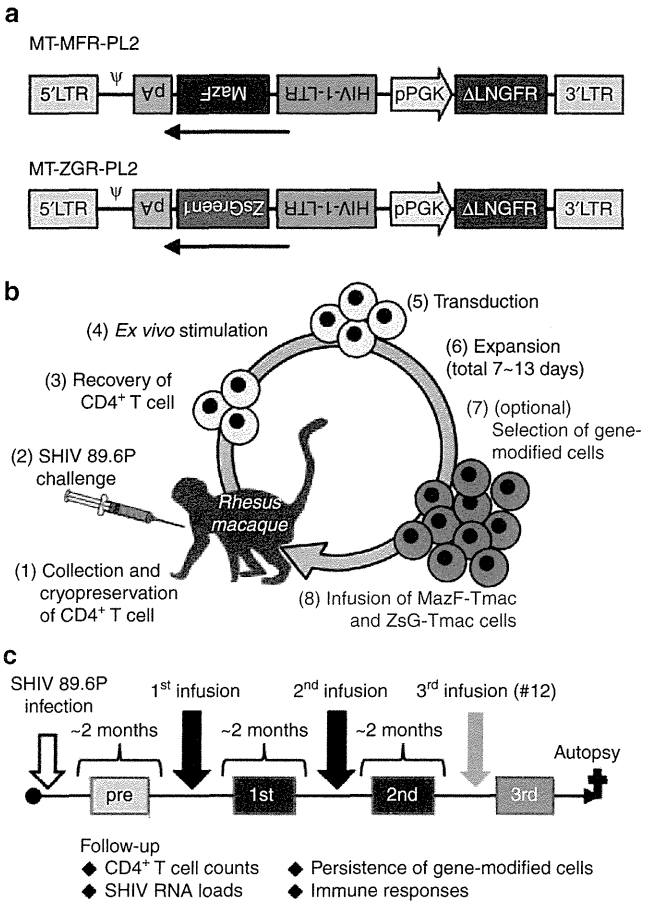

Figure 1 Diagram of autologous CD4+ T cell transplantation in a primate model. (a) Structures of the gamma-retroviral vectors MT-MFR-PL2 and MT-ZGR-PL2. LTR, long terminal repeat; MoMLV, Moloney murine leukemia virus; *LNGFR*, low-affinity nerve growth factor receptor gene; pPGK, phosphoglycerate kinase promoter. **(b)** Flow diagram of gene therapy in the rhesus macaques.[1] Peripheral blood was collected by apheresis; the CD4+ T cells were isolated and cryopreserved.[2] The rhesus macaques were challenged with SHIV 89.6P.[3,4] The CD4+ T cells were recovered and stimulated *ex vivo* with anti-CD3/CD28 beads.[5] The stimulated cells were transduced twice with retroviral vectors on days 3 and 4.[6] The transduced cells were expanded for an additional 3–9 days.[7] The ΔLNGFR-positive cells were selected at the second transplantation for rhesus macaques #13 and #15 and at the first transplantation for rhesus macaques #12 and #14.[8] On days 7–13, the expanded autologous cells were collected, washed and transplanted into the rhesus macaques intravenously. **(c)** Four rhesus macaques were transplanted with MazF-Tmac cells, and two were transplanted with control ZsG-Tmac cells. The rhesus macaques were followed over six months.

(>98%). More than 90% of these cells expressed CD95 and CD28, which are known markers of the central memory phenotype;[27] central memory cells generally have a longer lifespan than effector memory cells.[28] The expression levels of CXCR4, which is a known coreceptor for X4-tropic HIV-1 and SHIV entry, varied among animals and expansion periods.

Body weight and hematological data

There was no significant change in body weight throughout the experiment in the MazF-Tmac-transplanted rhesus macaques (see **Supplementary Figure S1a**). A gradual

Table 1 The summary of characteristics of gene-modified CD4+ T cells for each transplantation

	#12	#13	#14	#15	#16	#17
First transplantation						
Culture period (days)	13	9	13	9	9	9
Number of infused cells	2.1×10^9	3.0×10^9	2.3×10^9	1.6×10^9	1.6×10^9	1.1×10^9
CD271+ (gene-modified) (%)	97.2[a]	52.0	99.0[a]	54.1	53.8	75.0
CD3+ CD4+ (%)	98.3	99.9	99.0	99.8	99.2	99.8
CD28+ CD95+ CM (%)	93.4	97.5	95.4	98.7	N.D.	N.D.
CD28- CD95+ EM (%)	6.3	2.3	4.5	0.9	N.D.	N.D.
CXCR4+ (%)	36.3	63.2	8.9	65.5	67.9	52.6
Second transplantation						
Culture period (days)	9	13	9	13	10	10
Number of infused cells	2.7×10^9	3.3×10^9	1.8×10^9	2.7×10^9	3.8×10^9	2.8×10^9
Gene-modified (%)	69.5	96.3[a]	57.0	99.8[a]	55.2	75.7
CD3+ CD4+ (%)	99.0	99.9	98.7	99.8	99.5	99.6
CD28+ CD95+ CM (%)	96.9	90.8	97.7	97.6	N.D.	N.D.
CD28- CD95+ EM (%)	2.7	9.0	2.1	2.2	N.D.	N.D.
CXCR4+ (%)	55.4	47.8	35.7	84.0	63.5	63.4
Third transplantation						
Culture period (days)	7					
Number of infused cells	0.55×10^9					
Gene-modified (%)	65.4					
CD3+ CD4+ (%)	99.5					
CD28+ CD95+ CM (%)	96.9					
CD28- CD95+ EM (%)	3.1					
CXCR4+ (%)	77.0					

The autologous MazF-Tmac cells and the ZsG-Tmac cells were manufactured from the cryopreserved CD4+ T cells by stimulating the cells with anti-CD3/CD28 beads, and transducing them with the MT-MFR-PL2 and MT-ZGR-PL2 retroviral vectors. The CD3, CD4, CD28, CD95, CD271, and CXCR4 expression in the gene-modified cells at the time of transplantation were analyzed by flow cytometry.
[a]Gene-modified cells were concentrated based on their expression of the ΔLNGFR surface marker. CM, central memory; EM, effector memory; N.D., not determined.

decrease in body weight was observed in one ZsG-Tmac-transplanted rhesus macaque #16 by the end of the experiment (data not shown). Hematological data, including white blood cell count, hemoglobin concentration and platelets, were also analyzed, and significant changes were observed in rhesus macaque #16 at the end of the experiment (data not shown). Rhesus macaque #16 was sacrificed prior to the scheduled autopsy because of worsening symptoms. No significant changes were observed in any of the MazF-Tmac-transplanted rhesus macaques (see **Supplementary Figure S1b–d**). Thus, MazF-Tmac cells are considered safe based on the clinical observations.

CD4+ T cell counts in peripheral blood

To evaluate the impact of the autologous transplantation of gene-modified CD4+ T cells, the posttransplantation CD4+ T cell count values were compared with the values measured prior to transplantation. As shown in Figure 2a, the increases in the CD4+ T cell counts after transplantation of MazF-Tmac cells were significant in all four rhesus macaques, while no significant increases were observed in the two rhesus macaques transplanted with ZsG-Tmac cells. In the case of rhesus macaque #12, which was robustly infected with SHIV and had high viral loads (>10^5 copies/ml), the average CD4+ T cell count was 68 cells/μl before the gene therapy treatment, and increased to 107 cells/μl and 193 cells/μl after the first and second transplantation, respectively. Unfortunately, the mean CD4+ T cell count after the third transplantation decreased slightly to 139 cells/μl; this value was still higher than the baseline values.

The effectiveness was most clearly shown in the rhesus macaque #14, whose average CD4+ T cell count was 137 cells/μl before the gene therapy treatment, and subsequently increased to 329 cells/μl and 754 cells/μl after the first and second transplantations, respectively. To investigate the long-term safety of the treatment, this rhesus macaque was followed up for one and a half years. The other rhesus macaques (#13 and #15) had average CD4+ T cell counts of approximately 530 cells/μl before the gene therapy treatment that also increased to 1296 cells/μl and 856 cells/μl after the first transplantation, respectively, and retained these levels after the second transplantation. Thus, the transplantation of MazF-Tmac cells has the potential to increase CD4+ T cell counts.

Plasma SHIV viral loads

To investigate the influence of the transplantation of gene-modified cells, SHIV viral loads in the plasma were measured using quantitative PCR (qPCR). In rhesus macaque #15, the viral loads were below the detection limit at the time of gene therapy treatment. In rhesus macaques #13 and #14, the available data were limited to three time points due to a relatively short window in which they exhibited a stable set point before the infusion of MazF-Tmac cells. For this reason, we did not

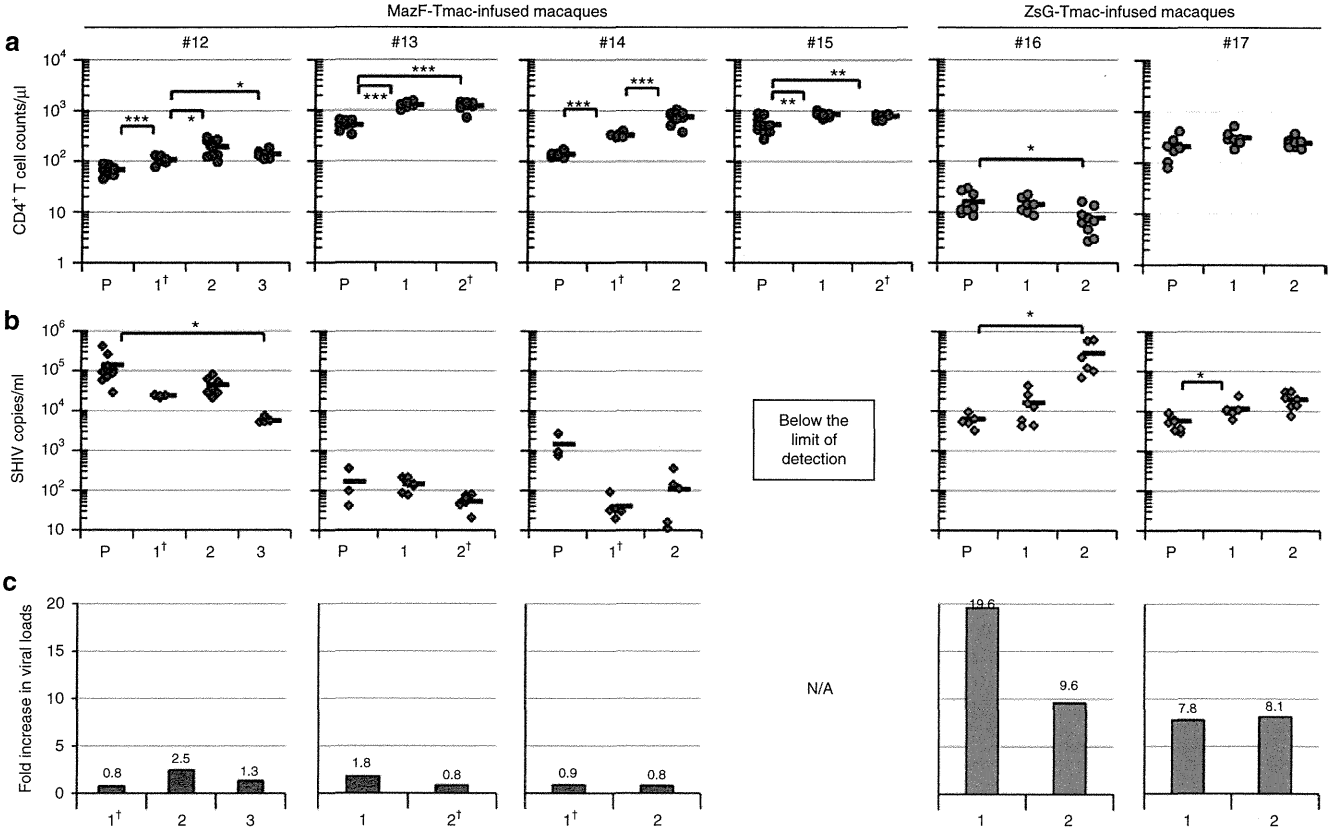

Figure 2 Changes in CD4⁺ T cell counts and viral loads. (a) The CD4⁺ T cell counts of MazF-Tmac- and ZsG-Tmac-transplanted rhesus macaques. The CD4⁺ T cell counts in the area of the viral load set point were averaged by multiple time point sampling 20 to 80 days after SHIV infection or transplantation. **(b)** Plasma SHIV viral RNA loads. The plasma SHIV viral RNA loads in the area of the set point were averaged by multiple time point sampling 20–80 days after SHIV infection or transplantation of gene-modified cells. **(c)** The fold increase of the plasma viral loads of MazF-Tmac- and ZsG-Tmac-transplanted rhesus macaques. The fold increase values were calculated by dividing [the average viral loads one week after transplantation of gene-modified cells] by [the average viral loads three weeks before transplantation of gene-modified cells]. P, pretransplantation of gene-modified cells; 1, after the first transplantation; 2, after the second transplantation; 3, after the third transplantation. Statistical significance indicated by Student's *t*-test (*$P < 0.05$; **$P < 0.01$; and ***$P < 0.001$). †Gene-modified cells were concentrated using the ΔLNGFR marker. N/A, not applicable due to undetectable viral loads.

employ statistical analyses between pre and postinfusion for these two macaques. However, there was no increase and tendency toward decrease in the viral loads after transplantation of MazF-Tmac cells (Figure 2b). For rhesus macaques #16 and #17, significant increases in the set point of SHIV viral loads were observed upon transplantation of ZsG-Tmac cells (Figure 2b). A dramatic rebound was detected immediately after transplantation (Figure 2c). These data indicate that the transplantation of ZsG-Tmac cells, which have no protective payload for SHIV, significantly impacted the viral loads. No remarkable rebound was observed after transplantation of MazF-Tmac cells (Figure 2c).

Longitudinal persistence of MazF-Tmac cells and ZsG-Tmac cells

To examine the *in vivo* persistence of transplanted MazF-Tmac cells and ZsG-Tmac cells, peripheral blood samples were collected to monitor the presence of gene-modified cells. The proviral copy number of the transduced retroviral vector was monitored by the qPCR method throughout the experiment. MazF-Tmac cells persisted for more than 6 months in the presence of SHIV. In particular, persistence for longer than one and a half years was observed in rhesus macaque #14. The ZsG-Tmac cells had nearly disappeared within two months after transplantation (Figure 3a). Similar results were obtained in flow cytometry analyses to detect the surface marker ΔLNGFR in the CD4⁺ T cells (Figure 3b). The calculated half-lives measured within 2 months of transplantation of the MazF-Tmac cells were much longer than that of the ZsG-Tmac cells (Table 2). The half-lives of the MazF-Tmac cells became even longer in the late phase of the experiment. Notably, in rhesus macaque #14, the half-life of the MazF-Tmac cells was 128.6 days when the period of analysis was extended to 9 months posttransplantation.

MazF antigen-specific interferon gamma (IFN-γ) enzyme-linked immunospot (ELISPOT) assay

To assess whether a cellular immune response was elicited by MazF-Tmac cells, an IFN-γ ELISPOT assay was performed. Peripheral blood mononuclear cells (PBMCs) from the MazF-Tmac-transplanted rhesus macaques were stimulated with a cocktail of MazF-overlapping peptides (see **Supplementary Figure S2**). As a negative control, PBMCs prepared from a normal (*i.e.*, untransplanted) rhesus

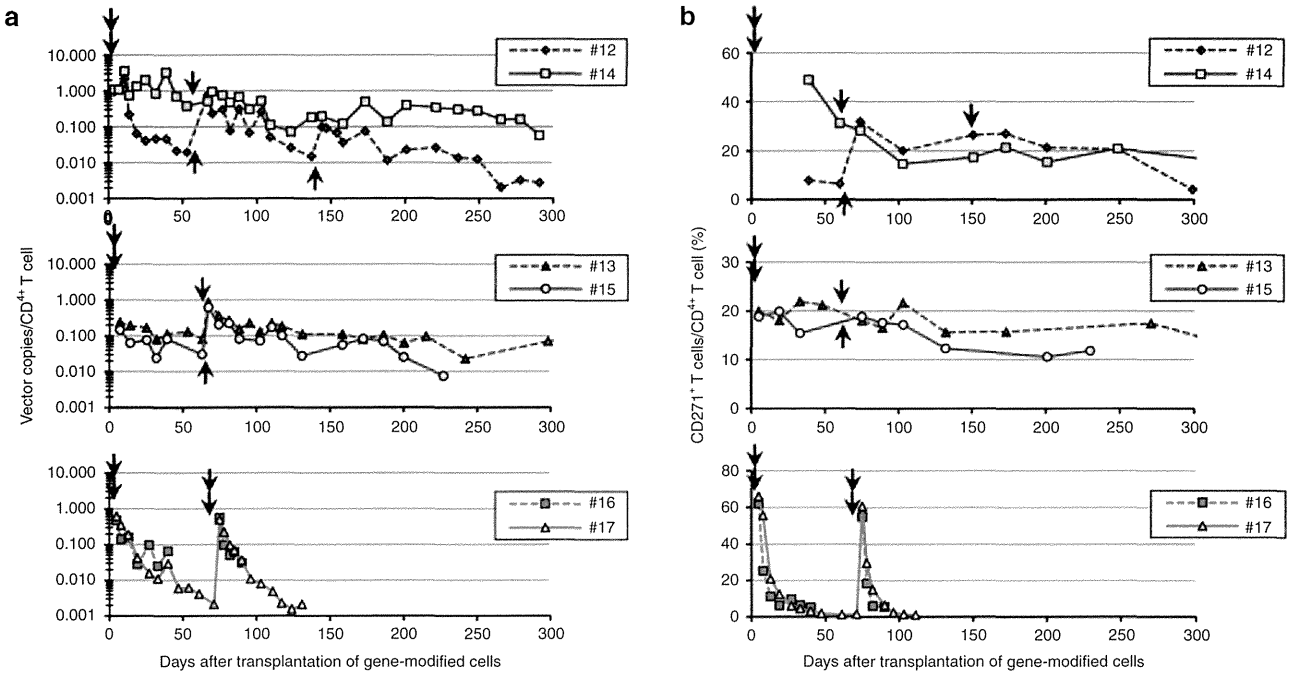

Figure 3 ***In vivo*** **persistence of MazF-Tmac and ZsG-Tmac cells. (a)** The persistence of MazF-Tmac cells and ZsG-Tmac cells was quantified using qPCR. The percentage of CD4+ T cells was analyzed using flow cytometry, and the proviral vector copy number was analyzed using qPCR. Using these data, the copy number of the transgene in CD4+ T cells was calculated. The arrows indicate the time point at which the gene-modified cells were transplanted. **(b)** The persistence of MazF-Tmac cells and ZsG-Tmac cells was quantified using flow cytometry. The percentage of gene-modified cells in the CD4+ T-cell population was determined after expanding the PBMCs with anti-CD3/CD28 beads stimulation for seven days, followed by antibody staining for CD4 and CD271 surface markers. The arrows indicate the time points at which the gene-modified cells were transplanted.

Table 2 The half-lives of gene-modified CD4+ T cells in each transplantation

	MazF-Tmac transplantation				ZsG-Tmac transplantation	
	#12	#13	#14	#15	#16	#17
First transplantation	7.7	42.8	35.6	32.4	3.9	4.6
Second transplantation	14.9	57.6	33.8	51.3	4.2	6.9
Third transplantation	29.0	N/A	N/A	N/A	N/A	N/A

The *in vivo* half-lives of the gene-modified cells in each rhesus macaque within a period of two months after transplantation was calculated by linear regression analyses using Microsoft Excel software.
N/A, not applicable.

macaque were stimulated. As shown in Figure 4a, no significant cellular immune responses related to the MazF-specific antigens were observed, indicating that the infused MazF-Tmac cells did not elicit a cellular immune response in the rhesus macaques in the presence of SHIV infection.

Detection of antibodies against MazF or ZsGreen1 in rhesus macaque blood

The evidence of longitudinal persistence of the MazF-Tmac cells supports the idea that these cells are not highly immunogenic; however, it is still important to assess the production of antibodies against MazF. As shown in Figure 4b, no significant production of antiMazF antibodies was detected in the blood samples from any of the rhesus macaques after transplantation with the MazF-Tmac cells. For the ZsG-Tmac cells, significant production of antibodies against ZsGreen1 was detected in rhesus macaque #17, while no antibody production was detected in rhesus macaque #16. The MazF-Tmac cells persisted for an extended period *in vivo*, and the MazF-Tmac-transplanted rhesus macaques produced no antibodies against MazF, indicating that the infused MazF-Tmac cells can be considered safe and not immunogenic in rhesus macaques in the presence of SHIV infection.

Distribution of gene-modified cells

At autopsy, lymphocytes isolated from several organs were analyzed for the distribution of the gene-modified cells using flow cytometry and qPCR. As shown in Table 3, ΔLNGFR-positive cells were detected by flow cytometry in the CD4+ T cells isolated from several lymph nodes, the spleen and the peripheral blood of the MazF-Tmac-transplanted rhesus macaques. A similar trend was observed in the qPCR analysis. The bone marrow, liver, and small intestine were also analyzed, but there were no detectable signs of gene-modified cells (data not shown). In the ZsG-Tmac-transplanted rhesus macaques, no gene-modified cells were detected in the organs or peripheral blood. These data strongly suggest that transplanted MazF-Tmac cells could circulate to the peripheral blood and the secondary lymphoid organs.

Histopathological analyses

It is advantageous to use primate models to investigate the safety of gene-modified cells because these animals can